Tectonics®

RESEARCH ARTICLE
10.1029/2019TC005990

Key Points:

- Broad, progressive terrace folding in the Obion River valley in the New Madrid seismic zone (NMSZ) is documented using lidar and auger data
- Folded terraces record Reelfoot fault slip since ≥24 ka, and historical lake records lengthen the 1812 earthquake rupture to ≥58 km
- The southern extent of the Reelfoot fault reaches at least the Obion River valley with a potential total fault rupture length of ≥70 km

Supporting Information:

Supporting Information may be found in the online version of this article.

Correspondence to:

J. E. Delano,
jaimedelano@gmail.com

Citation:

Delano, J. E., Briggs, R. W., Thompson Jobe, J., Gold, R. D., & Engelhart, S. E. (2021). Quaternary Reelfoot fault deformation in the Obion River valley, Tennessee, USA. *Tectonics*, *40*, e2019TC005990. https://doi.org/10.1029/2019TC005990

Received 18 NOV 2019
Accepted 2 AUG 2021

Quaternary Reelfoot Fault Deformation in the Obion River Valley, Tennessee, USA

Jaime E. Delano[1,2], Richard W. Briggs[1], Jessica Thompson Jobe[1], Ryan D. Gold[1], and Simon E. Engelhart[3]

[1]U.S. Geological Survey, Geologic Hazards Science Center, Golden, CO, USA, [2]University of Canterbury, Christchurch, New Zealand, [3]Department of Geography, Durham University, Durham, UK

Abstract Blind reverse faults are challenging to detect, and earthquake records can be elusive because deep fault slip does not break the surface along readily recognized scarps. The blind Reelfoot fault in the New Madrid seismic zone in the central United States has been the subject of extensive prior investigation; however, the extent of slip at the southern portion of the fault remains unconstrained. In this study, we use lidar to map terraces and lacustrine landforms in the Obion River valley and investigate apparent broad folding resulting from slip on the buried Reelfoot fault. We compare remote surface mapping results with three auger boreholes in the ~24 ka Finley terrace and interpret apparent warping as due to tectonic folding and not stratigraphic thickening. We combine our results with historical records of coseismic lake formation that indicate surface deformation dammed the Obion River in the 1812 CE earthquake. Older terraces (deposited at least 35–55 ka) record progressive fold scarps ≥1, ≥2, and ≥8 m high indicating a long record of earthquakes predating the existing paleoseismic record. Broad, distributed folding above the Reelfoot fault into the Obion River valley is consistent with a deep active fault tip along the southern reaches of the fault. Our analyses indicate the entire length of the fault (≥70 km) is capable of rupture and is more consistent with longer rupture scenarios.

Plain Language Summary Blind faults do not break the ground and often leave behind little evidence of earthquakes, making earthquake hazard estimates difficult. The blind Reelfoot fault in the central United States has produced large, damaging earthquakes as recently as 1812, but information about the earthquake size and fault rupture length is sparse, especially towards the southern fault tip. To better understand the southern fault, we use lidar to map river and lake deposits in the Obion River valley. These surfaces show wide warping caused by past earthquakes on the Reelfoot fault. Three boreholes in an abandoned river terrace show that folding also exists below the surface. We also present historical records of a lake that formed in the Obion River valley from the 1812 earthquake. Older terraces are folded more than younger terraces, meaning that earthquakes have been warping the surface for many thousands of years, longer than other earthquake records here. The surface folding is wider in the Obion River valley than farther north along the fault which implies deeper fault movement towards the south. Our results suggest the entire length of the fault (≥70 km) can produce large earthquakes, which is towards the upper range of existing hazard estimates.

1. Introduction and Motivation

Constraining the source faults of past earthquakes in intraplate settings, such as the New Madrid seismic zone (NMSZ) in the central United States, is key to quantifying seismic hazard (Petersen et al., 2014; U.S. Dept. of Energy, Electric Power Research Institute, and U.S. Nuclear Regulatory Commission, 2012). The NMSZ most recently produced three M7+ earthquakes during the winter of 1811–1812 CE (Nuttli, 1973) and at least four other strong shaking events in the last ~4,370 yrs (since ~2350 BCE) (Figure 1) (Gold et al., 2019; Holbrook et al., 2006; Kelson et al., 1996; Tuttle et al., 2002, 2005, 2019). Ambiguity in the magnitudes, source faults, rupture lengths, and slip amounts for the 1811–1812 earthquakes is due to both (a) a lack of seismic instrumentation in the region in 1811–1812 and (b) subsequent natural and anthropogenic landscape modification, which obscure geomorphic evidence of faulting and folding. These problems are accentuated for the longer-term earthquake record and hinder traditional paleoseismic investigations, such as fault trenching, in this region. On shorter time scales, multi-decadal regional geodetic observations show

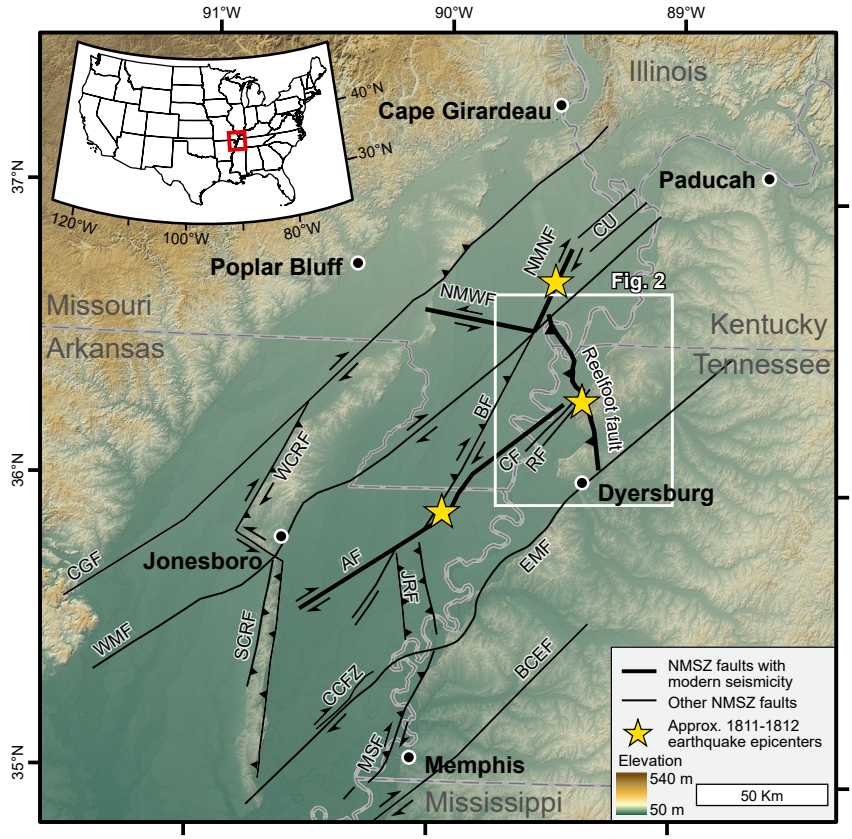

Figure 1. Overview of the New Madrid seismic zone and major structures in the Mississippi Embayment. Largest 1811–1812 earthquake epicenters from Bakun and Hopper (2004). Fault mapping modified from Hao et al. (2013), Johnston and Schweig (1996), Martin and Hough (2019), Stephenson et al. (1995), and Thompson Jobe et al. (2020). Teeth indicate dip direction of a reverse fault; arrows indicate sense of strike-slip. Gray lines are state boundaries. AF = Axial fault; BCEF = Big Creek-Ellendale fault; BF = Bootheel fault; CCFZ = Crittenden County fault zone; CF = Cottonwood Grove fault; CGF = Commerce Geophysical fault; CU = Charleston Uplift; EMF = Eastern Margin fault; JRF = Joiner Ridge fault; MSF = Meeman-Shelby fault; NMNF = New Madrid North fault; NMWF = New Madrid West fault; RF = Ridgely fault; SCRF = Southern Crowleys Ridge fault; WCRF = Western Crowleys Ridge fault; WMF = Western Margin fault.

near-zero deformation rates (e.g., Calais & Stein, 2009; Calais et al., 2006), which can conceal potential fault activity and further challenge seismic hazard estimates.

The blind Reelfoot reverse fault was one source of the 1811–1812 New Madrid earthquake sequence and is one of the few faults east of the Rocky Mountains with documented Holocene surface expression (Fisk, 1944; Fuller, 1912; Mueller & Pujol, 2001; Russ, 1979, 1982; Van Arsdale et al., 1995). A key outstanding question for NMSZ hazard models is how far the Reelfoot fault extends to the south. The length of the Reelfoot fault has important implications for potential rupture length, slip area, and estimated seismic hazard of the region (Mueller & Pujol, 2001; Petersen et al., 2014). Previous seismological studies recognize modern microseismicity on the Reelfoot fault that extends as far south as Dyersburg, Tennessee (Figure 2) (Greenwood et al., 2016; Mueller & Pujol, 2001; Van Arsdale et al., 1995). Evidence of clear coseismic surficial fault deformation has only been observed along the northern extent of the Reelfoot fault near Reelfoot Lake (Greenwood et al., 2016; Van Arsdale et al., 1998) and within the Mississippi River terraces (Figure 2) (Holbrook et al., 2006). Farther southeast in the bluffs, geomorphic, geophysical, and geological studies infer broad uplift or slip at depth on the Reelfoot fault in the Tertiary and Quaternary, but do not identify a fault scarp on the surface (Delano et al., 2018; Greenwood et al., 2016; Gold et al., 2019; Van Arsdale et al., 1998). Near the Obion River (Figure 2), sparse observations and inconclusive or conflicting interpretations of surface deformation leave room for debate regarding the southernmost extent of past Reelfoot fault rupture (Rodbell et al., 1997; Van Arsdale et al., 1999).

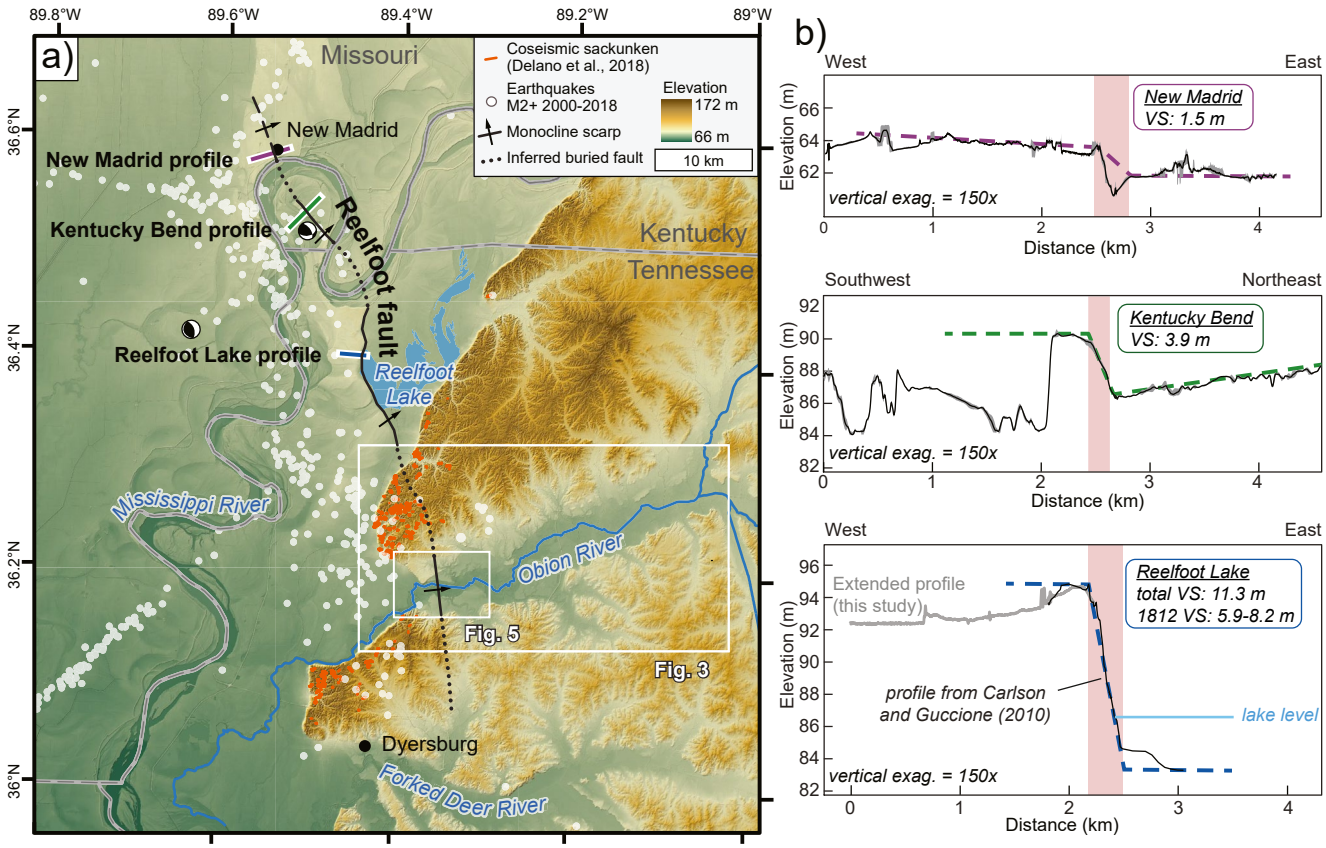

Figure 2. Location and expression of the blind Reelfoot fault. (a) Extent of the surface projection of the Reelfoot fault with locations of modern seismicity (CERI, 2019) and example focal mechanisms (Johnson et al., 2014), Reelfoot fault fold-scarp profiles, and coseismic sackungen (Delano et al., 2018). The blind Reelfoot fault is expressed at the surface as a monoclinal fold—solid lines indicate a clear fold scarp, dotted lines indicate eroded fold trace, dashed where location is approximate and diffuse. (b) Topographic profiles of folding above the northern section of the Reelfoot fault. Gray polygon ranges from minimum to maximum values within 40-m-wide swath; black line is the average elevation. Red shaded boxes represent the location and width of the monocline forelimb, which is relatively narrow along this section of the structure. The fold scarp amplitude increases toward the center of the Reelfoot fault. The Reelfoot Lake profile includes topographic data from Carlson and Guccione (2010) and is extended with lidar digital elevation models from this study. The red box is the approximate projection of the monocline forelimb above the blind Reelfoot fault.

This study uses newly available airborne lidar to evaluate evidence of fault slip on the Reelfoot fault in western Tennessee (USACE, 2012; USGS, 2014). We combine findings from lidar-derived bare earth digital elevation models (DEMs) and auger-based stratigraphic observations from late Quaternary surfaces with past research and historical records. These new data are used to shed light on fault behavior near the southern extent of the Reelfoot fault and to assess the relative contribution of tectonic deformation and climate-driven processes recorded by landforms in the Obion River valley. We interpret the surfaces to record evidence of deformation related to blind slip along the Reelfoot fault in the Obion River valley, expanding our understanding of past earthquakes on the Reelfoot fault to better characterize seismic hazard in the region.

2. Geologic Setting

2.1. New Madrid Seismic Zone

The NMSZ occupies the northern Mississippi Embayment spanning northwestern Tennessee, southeastern Missouri, northeastern Arkansas, and southwestern Kentucky (Figure 1). The 1811–1812 historical earthquake sequence in the NMSZ is characterized by three main shocks: the first and second earthquakes likely occurred on northeast-striking, right-lateral strike-slip faults (Figure 1) (Bakun & Hopper, 2004). The third event on February 7, 1812 occurred on the Reelfoot fault, a southeast-striking reverse fault that accommodates contraction between the two strike-slip faults (Figure 1) (Bakun & Hopper, 2004; Pratt, 2012).

Modern seismicity and geophysical surveys suggest that the SSE-striking Reelfoot fault extends 60–80 km from approximately 6 km northwest of New Madrid, Missouri, to approximately Dyersburg, Tennessee (Figure 2) (Greenwood et al., 2016; Van Arsdale et al., 1999). The Reelfoot fault is commonly split into northern and southern sections, defined by the intersection with the Cottonwood Grove and Ridgely faults (Figure 1) (Csontos & Van Arsdale, 2008; Greenwood et al., 2016; Van Arsdale et al., 2013). Previous identification of Quaternary surface deformation along the Reelfoot fault is limited to the northern section of the fault, but preservation is complicated by the migrating Mississippi River. The 1812 earthquake on the Reelfoot fault generated a broad, monoclinal scarp that, together with footwall subsidence, dammed the Reelfoot River, flooded the lowlands upstream, and created Reelfoot Lake (Figure 2) (Fuller, 1912; Russ, 1982; Stahle et al., 1992). The fold scarp bounding Reelfoot Lake is typically considered the southernmost extent of surface deformation from the 1812 event on the Reelfoot fault, although the fold scarp may have extended southeast to the bluff margin and has subsequently been eroded (Greenwood et al., 2016).

The southern section of the Reelfoot fault extends southeast from the Mississippi River floodplain margin into a region of elevated, dissected ridges (bluffs) with 35–50 m of relief above the lowlands (Figures 1 and 2a). Prior to this study, evidence for the blind Reelfoot fault southeast of Reelfoot Lake was limited to broader signals of uplift, coseismic sackungen (ridgetop gravitational failures), or folding at depth in seismic surveys. For example, Greenwood et al. (2016) interpret ~6 m of distributed uplift above the Reelfoot fault since ~10 ka from small abandoned terraces in minor drainages within the bluffs, and Van Arsdale et al. (1999) highlight a local drainage divide that occurs subparallel to the trend, and within the upthrown side, of the southern projection of the Reelfoot fault. Remote mapping studies and trenching investigations of sackungen in the bluffs within 15 km of the Reelfoot fault suggest the southern section of the Reelfoot fault has experienced repeated large earthquakes since 11 ka (Figures 2a and 3a) (Delano et al., 2018; Gold et al., 2019). Seismic surveys along the bluff margin (Greenwood et al., 2016) and northern edge of the Obion River valley (Van Arsdale et al., 1999) reveal folding in Tertiary sediments within 120 m of the surface (Figure 3a). The coseismic sackungen identified in Delano et al. (2018) extend south from the bluff margin to nearly Dyersburg, Tennessee (Figure 2a), suggesting that recent (<11 ka) movement on the Reelfoot fault extended south of the Obion River valley.

2.2. Stratigraphy and Geomorphology of the Obion River Valley

The Obion River flows westward from the bluffs and enters the Mississippi River floodplain north of Dyersburg, Tennessee (Figures 2a and 3a). The lower Obion River valley consists of a single, southwest-draining channel; the upper reaches are comprised of four smaller tributaries that merge to form the lower Obion River ~35 km northeast of the Mississippi River valley margin. The bluffs flanking the Obion River are underlain by sub-horizontal or gently dipping marine sedimentary Eocene Jackson Formation (Conrad, 1856) and fluvial sand and gravel of the Plio-Pleistocene Upland complex (Autin et al., 1991). The bluffs are capped by 5–50-m-thick Pleistocene loess derived from successive glacial outwash deposits in the Mississippi River valley (Autin et al., 1991; Markewich et al., 1998; Rodbell et al., 1997). These loess deposits generally decrease in thickness to the east with increasing distance from the Mississippi River valley (Autin et al., 1991; Rodbell et al., 1997). The entire region, both in the valleys and in the bluffs, has long-lived and ongoing agricultural development, such as farming and logging, which has contributed to surface modification since the 1812 earthquake.

Three previously identified terraces in the Obion River valley include the Finley terrace (~24 ka), the Hatchie terrace (older than 35–55 ka), and the Humboldt terrace (pre-Wisconsin), although map depictions of the terraces vary (Rodbell, 1996; Saucier, 1987). These terraces are remapped in this study (Figure 3b and Plate S1). An additional older, undated terrace (Henderson terrace) was identified in the adjacent Forked Deer drainage (Figure 2) (Saucier, 1987), but had not been identified in the Obion River valley prior to this study. Three loess deposits in the Obion River valley provide minimum ages for the underlying terraces: the Peoria Loess (10–25 ka) (McKay, 1979; Ruhe, 1983), Roxana Silt (35–55 ka) (Forman et al., 1992; Leigh & Knox, 1993; Markewich et al., 1998; Rodbell et al., 1997), and Loveland Loess (70–120 ka) (e.g., Forman & Pierson, 2002; Markewich et al., 1998; Rodbell et al., 1997). The Finley terrace is mantled by ~2–4 m of Peoria Loess, and the Finley terrace abandonment age (~24 ka) was previously constrained by two radiocarbon ages at different locations—charcoal fragments in the overlying Peoria Loess and gastropod shells

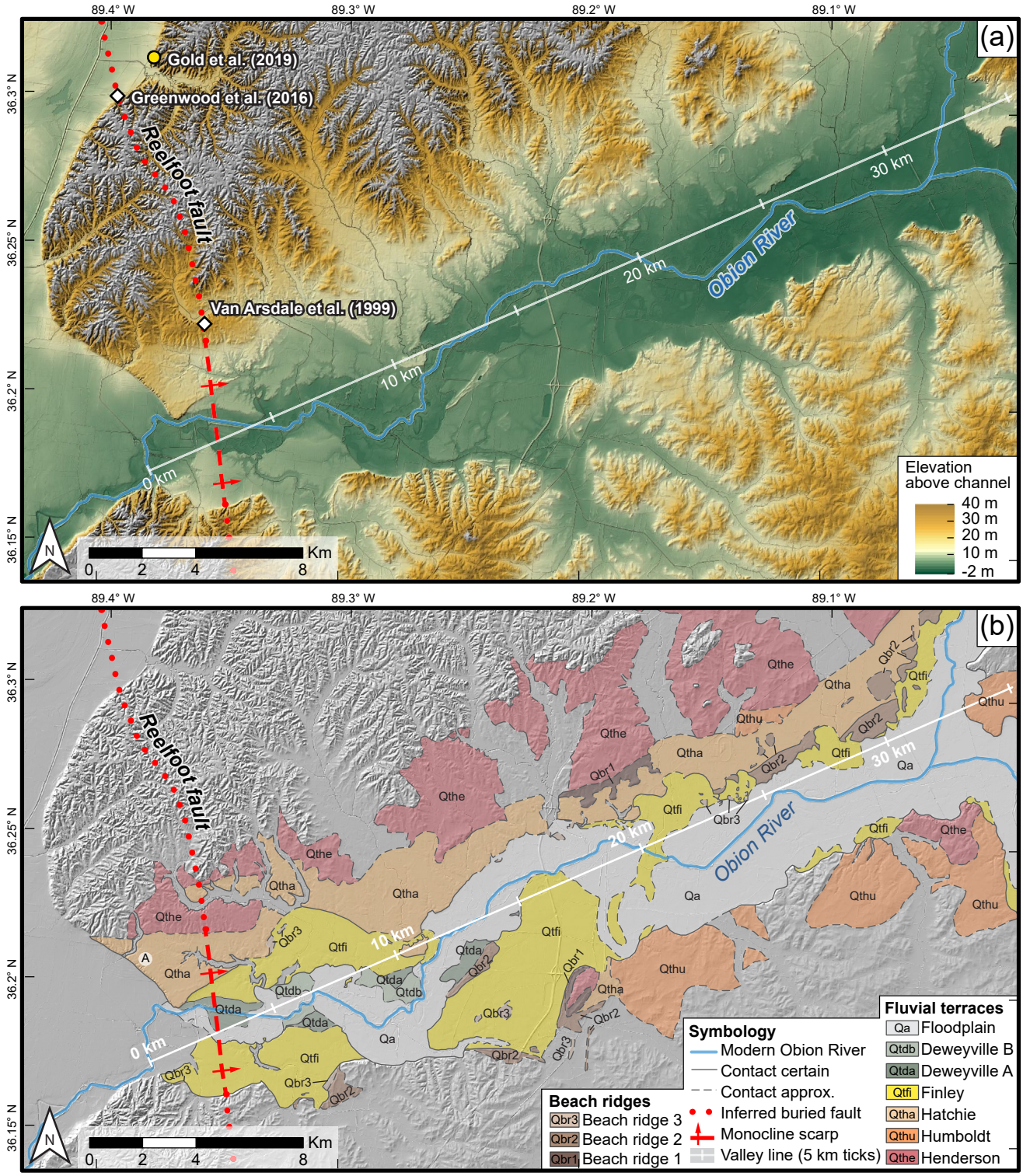

Figure 3. Obion River valley and surface projection of the blind Reelfoot fault—dotted lines indicate eroded fold scarp or inferred surface projection, dashed where fold scarp is diffuse. White line shows valley distance used in Figure 4. See Figure 2 for location. (a) Relative elevation model of the lower Obion River valley where the modern channel represents base elevation level. The modern floodplain constricts from upstream (east) to downstream (west) suggesting uplift in the lower reaches of the valley. Diamonds are seismic surveys that constrain fault location, yellow dot is sackung trench location (Gold et al., 2019). (b) Geomorphic mapping of the lower Obion River valley. Marker A referenced in text.

from the terrace alluvium (Rodbell, 1996; Rodbell & Schweig, 1993). The timing of Hatchie and Humboldt terrace abandonment is constrained by minimum ages from the capping loess deposits—both are mantled by Roxana Silt and Peoria Loess, suggesting they are both older than 35–55 ka (Forman et al., 1992; Leigh & Knox, 1993; Markewich et al., 1998; Rodbell et al., 1997). Total loess thickness on the Hatchie and Humboldt terraces is spatially variable and poorly constrained; investigations in the Obion River valley did not establish the contact between loess and terrace deposits (Rodbell, 1996; Rodbell, et al., 1997).

Terraces in the Mississippi River and Obion River valleys have been interpreted as a series of landforms recording base-level change caused by interrelated processes including (a) glacio-eustatic variation in sea level; (b) spatiotemporal variation in sediment yield linked to climate change; and (c) regional tectonics, including subsidence (Autin et al., 1991). When viewed in this regional framework, Obion River terraces at the valley mouth may largely record local base-level increases from rapid sedimentation in the adjacent Mississippi River valley resulting in sediment influx and backwater flooding into the Obion River valley (Autin et al., 1991). The observation that each Obion River terrace is mantled by loess from the corresponding Pleistocene glacial retreat (Autin et al., 1991; Rodbell, 1996) provides circumstantial support for the interpretation that lower Obion River terraces are heavily influenced by Mississippi sedimentation and thus climatically driven changes in local base level (Autin et al., 1991).

Two primary landforms—horizontal-gradient terraces and constructional shorelines—are consistent with pronounced local base-level change at the mouth of the Obion River. Saucier (1987) previously observed that both the Finley and Hatchie terraces have a near-zero gradient in the lower reaches of the Obion River valley (Saucier, 1987). In addition to the terraces, Saucier (1987) mapped a series of discontinuous beach ridges and interpreted them as lacustrine shoreline features. The gentle gradient of the Obion river-mouth terraces and shorelines record tributary drowning and lake formation; previously, this geomorphic record was interpreted as tied solely to regional base-level changes propagating along the Mississippi River valley (Autin et al., 1991; Saucier, 1987; Saucier & Fleetwood, 1970).

Previous studies also noted that the Finley, Hatchie, and possibly Humboldt terraces have slight reverse gradients near the confluence of the Obion River and the Mississippi River valleys (Rodbell, 1996; Saucier, 1987; Van Arsdale et al., 1999). Here, the terrace elevations deviate vertically from projected river gradients by ~3 m for the Finley terrace (Rodbell, 1996; Saucier, 1987), ~10 m for the Hatchie terrace, and ~12 m for the Humboldt terrace (Rodbell, 1996). These reverse gradients have been interpreted as sediment introduction from the Mississippi River during backwater flooding (Saucier, 1987), a reflection of the regional westward-thickening loess mantle (Rodbell, 1996), or a response to tectonic deformation (Van Arsdale et al., 1999).

In addition to the terrace tread reverse gradients, Van Arsdale et al. (1999) recognized several possible indicators of tectonic deformation in the Obion River valley. A slight reverse gradient in the Holocene floodplain stratigraphy, as interpreted from coring data, might represent broad folding above the blind Reelfoot fault (Van Arsdale et al., 1999). Stream migration vectors and a drainage divide in the surrounding bluffs near the projected trace of the Reelfoot fault are also consistent with distributed tectonic uplift (Van Arsdale et al., 1999). Additionally, the modern Obion River floodplain narrows down valley, which could reflect uplift near the valley mouth (Van Arsdale et al., 1999). Finally, Van Arsdale et al. (1999) noted one historical map (Rhea, 1832) that displays a prominent lake within the Obion River valley postdating the 1812 earthquake on the Reelfoot fault; they suggested that the lake may have formed as a result of river damming from uplift on the hanging wall of the Reelfoot fault, similar to Reelfoot Lake 20–25 km to the northwest. Currently, only portions of the lower Obion River valley flood seasonally and no long-standing lakes exist. The valley floor and river channel, however, have experienced extensive anthropogenic modification over the 20th century, including channelization, widening, dredging, levee creation, and farming (Simon & Hupp, 1992).

3. Methods

3.1. Geomorphic Mapping Methods

To more fully explore the hypothesis that the Obion River valley records tectonic deformation (Van Arsdale et al., 1999), we use a combination of lidar-derived DEMs, slope and hillshade maps, and relative elevation

models (REMs) to delineate terraces and other landforms. The REM represents elevation as height above the modern Obion River channel and removes elevation changes associated with the modern valley gradient (Olson et al., 2014). The 4-m-resolution REM was generated following the kernel density method outlined in Olson et al. (2014).

Terrace mapping was performed at ~1:10,000 scale (Figure 3b and Plate S1). We identify potential terraces by searching for planar surfaces with a gentle slope that contain a scarp at the contact with topographically higher and lower units. Terraces were differentiated by comparing relative tread elevations along and across the Obion River valley, tread elevations above the modern channel, and degree of tread dissection. The mapping extent in this study reaches from the eastern edge of the Mississippi River valley (bluff margin) to the confluence of the major Obion River tributaries ~30 km upstream, where the variable gradients, catchment areas, and discharge complicate terrace formation and preservation. We restrict mapping to the primary Obion River valley and truncate terrace mapping at tributaries on the northern and southern valley flanks.

3.2. Topographic Analysis Methods

To evaluate terrace trends and changes across the length of the lower Obion River valley, we generate valley longitudinal profiles for each mapped unit. We selected the best-preserved locations within each unit by avoiding areas obviously impacted by post-depositional incision, aggradation (e.g., alluvial fan) or anthropogenic modification (e.g., regrading). We then projected these point elevations to a central valley line and plotted the elevations as a function of valley distance upstream (referred to henceforth as "valley distance") (Figures 3 and 4). Some slight elevation variations within the same unit remain and are caused by incision, alluviation from tributaries, or variation in loess thickness.

We extract 40-m-wide swath elevation profiles from 1-m lidar-derived DEMs using Quick Terrain Modeler to compare the surface expression of the Reelfoot fault monocline along strike (Figures 2 and 5). The final 40-m-wide profile locations were chosen to (a) cross the mapped fault projection approximately orthogonally, (b) minimize effects of post-depositional incision, and (c) avoid anthropogenic alteration such as levees or agricultural regrading. The incised and eroded channel-migration topography leads to uncertainty in reconstructing surfaces across the monocline. To better capture this reconstruction uncertainty, we measure vertical separation by repeatedly projecting (~5 times) different combinations of up-and down-thrown surfaces to the scarp midpoint (i.e., DuRoss et al., 2019) (Figure 2). This method generates a range of plausible values, as well as a subjective best-fit preferred value, that represent uncertainty caused by several possible reconstructions of surfaces across the fold scarp. The New Madrid and Kentucky Bend profiles (Figure 2) in the Mississippi River floodplain, as well as Profiles *X* and *Y* on the Hatchie and Finley terraces (Figure 5), are drawn orthogonal to the surface projection of the Reelfoot fault trace. Profile *Z* on the Deweyville A terrace is projected to a line orthogonal to the mapped fault projection to account for surface modification by a modern levee. We did not include profiles from the Humboldt and Henderson terraces, because they either do not cross the surface projection of the Reelfoot fault or are too incised to reveal meaningful values.

3.3. Borehole Methods

In March 2018, we collected sediment from three 6- to 7-m-deep, hand-auger boreholes on the Finley terrace at the Wilson Loop (WL), Lanesferry (LF), and Biggs Farm (BF) sites (locations in Figure 5b). The goal of this limited borehole transect was to determine how subsurface stratigraphy changes across the Reelfoot fault monocline by tracking the loess thickness and underlying contact with the alluvium. We targeted sites along a profile nearly orthogonal to the monocline trend and chose three borehole locations to best capture the apparent inflection in the Finley terrace surface. Specific sites were chosen based on minimal post-depositional incision, low anthropogenic modification (such as significant regrading), and accessibility. We recovered each 20-cm boring increment from the soil auger bit, tracked depths for each increment, and examined sediment in the field. We estimate the uncertainty in depths as half the length of the soil auger bit, or ~10 cm. We made field observations of grain size, color, texture, structure, soil development, mineral deposits, moisture, and presence of organic/biological material as a function of depth. We also collected samples for additional analyses every 20 cm. We performed grain size analysis on 50 samples using a Malvern Mastersizer 3000. Samples were treated with hydrogen peroxide to remove organics and treated with

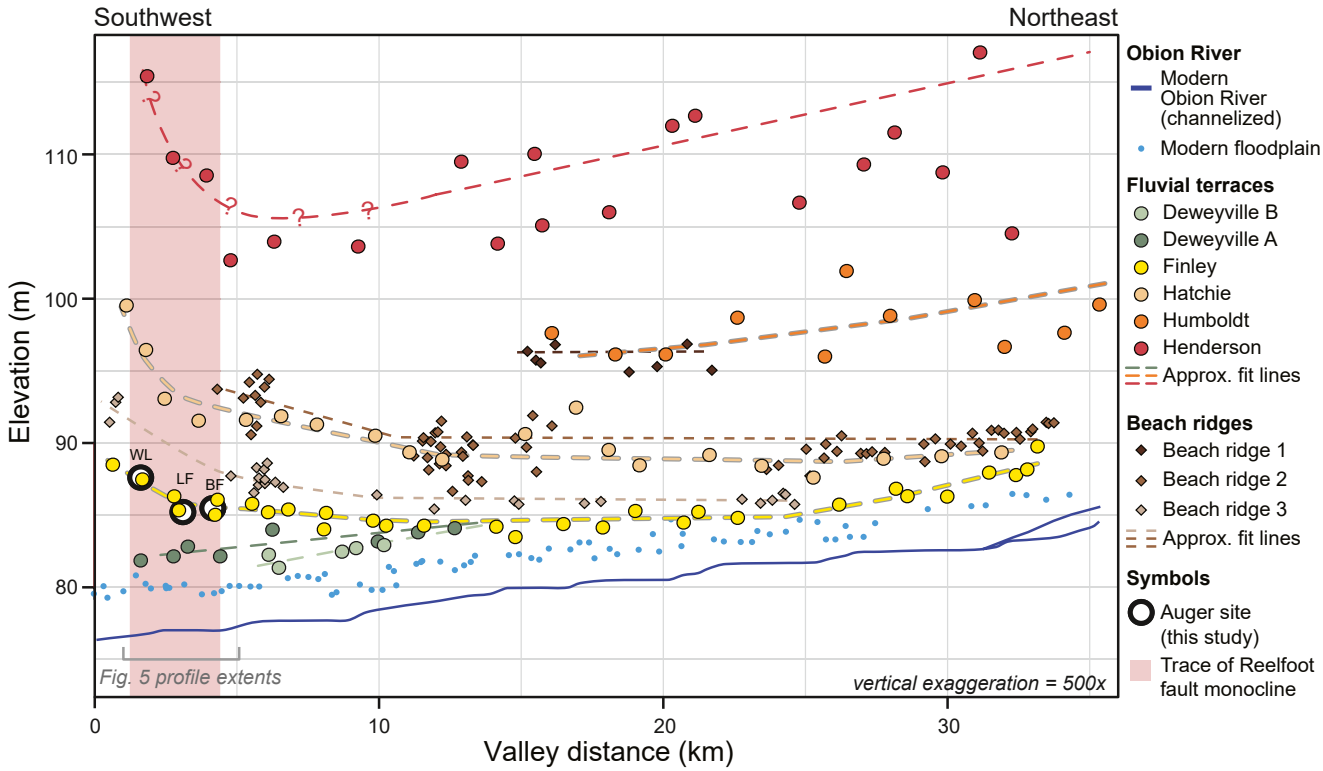

Figure 4. Longitudinal valley profiles of Obion River terraces and beach ridge complexes. Geomorphic features are projected orthogonal to a central valley line (see Figure 3). The Finley and Hatchie terraces and beach ridges 2 and 3 show apparent folding across the surface trace of the Reelfoot fault. The Henderson terrace may be warped across the fault, but incomplete preservation and post-depositional erosion make the relationship less clear. The horizontal gradients of the Finley and Hatchie terraces indicate a lacustrine-influenced origin. WL = Wilson Loop; LF = Lanesferry; BF = Biggs Farm.

sodium hexametaphosphate as a deflocculant. We quantified the relative percentages of each Wentworth grain size class (Wentworth, 1922). Complete field observations and analysis results of each auger site can be found in Tables S1–S7 in the companion data repository (Delano et al., 2021).

We attempted to identify mineralogical changes with depth using smear slides under a petrographic microscope, but the mineralogy between the loess and underlying alluvium is nearly identical, as found by previous studies (Snowden & Priddy, 1968). However, we note a sharp increase in carbonate content at 4.0 m depth in all three boreholes. We attribute this change in mineralogy to the pedogenic transition from carbonate leaching to carbonate precipitation, rather than a depositional change, consistent with observations of Snowden and Priddy (1968) at the same depth (13 feet). We also attempted to investigate potential changes in freshwater diatoms between the loess and terrace alluvium. Although the modern floodplain deposits contained freshwater diatoms, the samples retrieved from the boreholes did not preserve diatoms sufficient to use in this stratigraphic analysis (Dura, written communication, 2018).

Identifying stratigraphic changes and contacts within the loess and alluvium is complicated by the fact that (a) loess is typically fairly homogenous silt; (b) alluvium in this low-energy environment is predominantly silt and likely contains reworked loess; (c) the upper ~0.5 m is disturbed by plowing and other activity, removing near-surface structure; and (d) the high water table masks subtle features such as soil structure. We expect loess should be nearly all silt-sized grains, with potentially some finer-grained material in the near surface due to soil processes, while alluvium could be a mix of bedded clay, silt, and sand. Below, we summarize the observations and identify the most probable contact location using combined observations of subtle changes in grain size, color, structure, and macrofossils. At all three sites, grain size was the primary distinguishing feature between deposit types with additional changes recorded in the other characteristics. In some instances, characteristics other than grain size (such as color, structure, or fossils) were used to infer a contact because they heavily imply a change in depositional environment, even when grain size

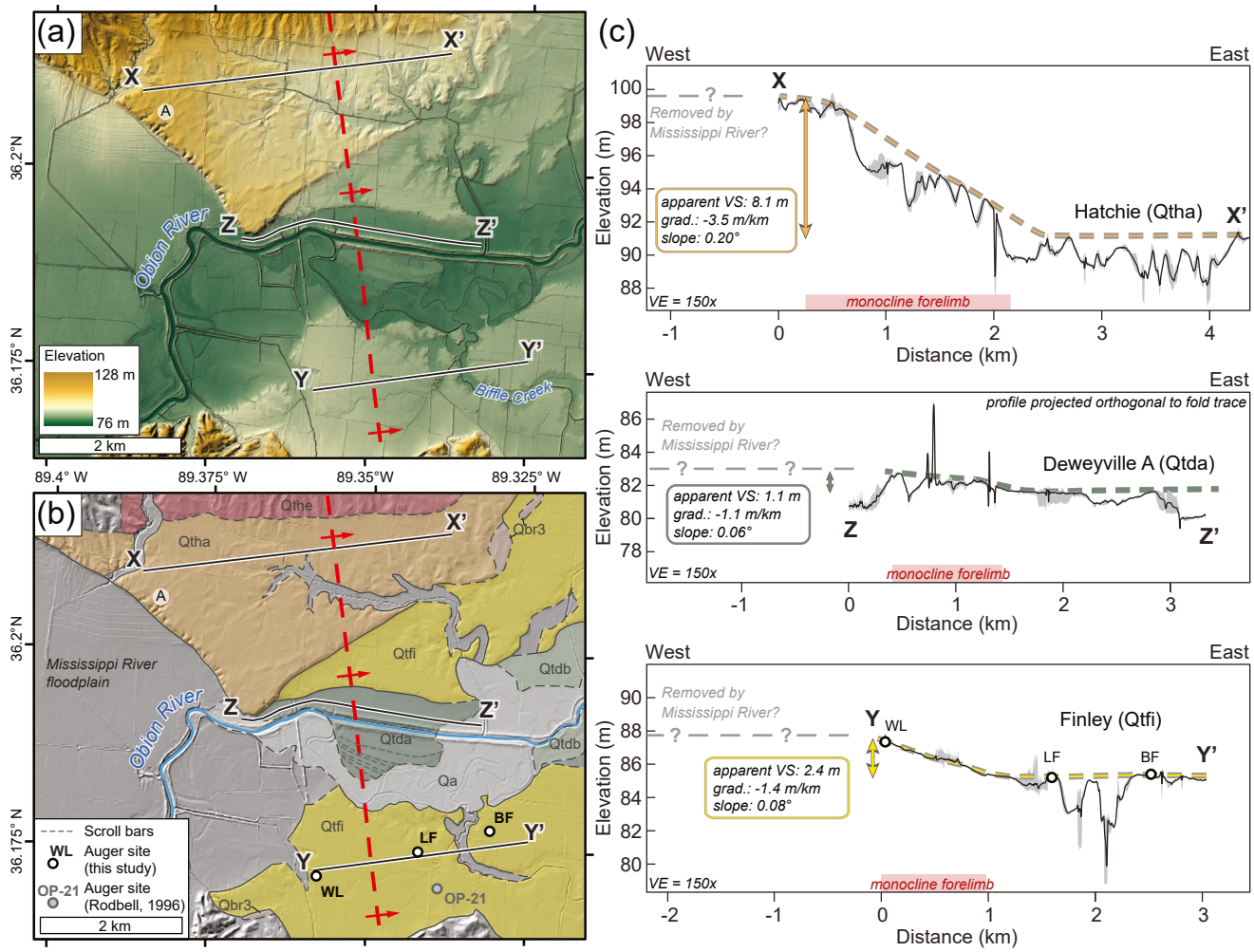

Figure 5. Location and expression of apparent warping above the blind Reelfoot fault in the Obion River valley (see Figure 2 for location). Marker A referenced in text. (a) Uninterpreted DEM of the Obion terraces across the Reelfoot fault monocline. (b) Geomorphic mapping of terraces across the Reelfoot monocline scarp showing auger sites and previous coring locations; map units and symbols same as in Figure 3. (c) Elevation profiles of warped terraces above the blind Reelfoot fault. Gray polygon ranges from minimum to maximum values within 40-m-wide swath; black line is the average elevation. The reverse (flow to the east) gradient/slope and vertical separation increases with terrace age. The monocline forelimb above the Reelfoot fault is much wider here than farther north (see Figure 2). The full extent of deformation is not recorded because the terraces have been truncated by Mississippi River erosion; possible reconstructions of eroded terraces as gray dashed and queried lines. WL = Wilson Loop; LF = Lanesferry; BF = Biggs Farm.

remained relatively uniform. Because grain size samples were taken at ~20 cm (and occasionally larger) intervals, we use changes in Munsell color and stratigraphic observations (e.g., appearance of laminations or fossils) to estimate contact placement between sample locations and corresponding changes in grain size.

3.4. Dating Methods

We performed accelerator mass spectrometry (AMS) radiocarbon dating of the snail shells to determine the age of the terrace sediment at the U.S. Geological Survey Radiocarbon Laboratory in Denver, Colorado. The clean, dry gastropod shells were broken and examined under a dissecting microscope to ensure that the interior whorls were free of secondary carbonate and detritus. Next, shells were bleached with 30% H_2O_2 to remove organic matter and etched with dilute HCl to remove 30%–50% of the total mass prior to hydrolysis (H_2O_2/HCl). Shell carbonate was then converted to CO_2 using American Chemical Society (ACS) reagent grade 85% H_3PO_4 under vacuum at 80°C until the reaction was visibly complete (~1 h). Water vapor and other contaminant gases (including SOx, NOx, and halide species) were removed from the sample CO_2 by

precise cryogenic separation at −140°C using a variable temperature trap capable of holding temperatures to within 1–2°C of the desired target. The resulting purified CO_2 gas was measured manometrically, converted to graphite using an iron catalyst and the standard hydrogen reduction process Vogel et al., 1984, and submitted for AMS ^{14}C analysis. We calibrated the radiocarbon ages using CALIB 8.2 (Stuiver et al., 2021) and the IntCal20 calibration curve for terrestrial samples (Reimer et al., 2020). Calibrated ages are presented at the 95% (2-sigma) confidence level.

4. Results

4.1. Fluvial Terraces

We mapped the Holocene floodplain, five progressively older terraces, and a series of beach ridges in the Obion River valley (Figure 3b, Plate S1, Delano et al., 2021). Terrace names are primarily derived from previous mapping within the Obion River valley by Saucier (1987) and newly mapped terraces (e.g., Deweyville complex and Henderson terrace) are named after equivalent terraces mapped in other nearby drainages. Elevations from the DEMs are reported relative to North American Vertical Datum of 1988. We mapped the following terrace units, listed youngest to oldest: Holocene floodplain (Qa), Deweyville complex (Qtdb and Qtda), Finley terrace (Qtfi), Hatchie terrace (Qtha), Humboldt terrace (Qthu), and Henderson terrace (Qthe). First, we present results of mapping and boreholes along the Finley (Qtfi) terrace, because it provides the clearest evidence for tectonic surface deformation near the mouth of the Obion River valley. We then present mapping and evidence from other terraces from youngest to oldest.

4.1.1. Finley Terrace

The Finley terrace surface (Qtfi) is minimally dissected and has distinct, sharp risers (Figure 3). At the western edge of the Obion River valley, the Finley terrace tread is 5–8 m above the modern floodplain but gradually decreases in relative height to 1–2 m above the modern floodplain at valley distances >15–18 km (Figure 4). The Finley terrace tread does not display migrating channel morphology, such as scroll bars or oxbow lakes, which likely reflects burial by Peoria Loess (Rodbell, 1996). In longitudinal profile, the Finley terrace surface has a reverse (northeast) gradient of 1.4 m/km (0.08°) from 0–3 km up the valley (Figure 5), a slight reverse gradient of 0.4 m/km (0.02°) at valley distances 3–10 km, a near-horizontal gradient at 10–24 km valley distance, and parallels the modern floodplain and channel gradient (0.4 m/km [0.02°] to the southwest) at valley distances >24 km (Figure 4).

4.1.1.1. Wilson Loop (WL) Soil Auger Borehole and Subsurface Stratigraphy

The Wilson Loop (WL) auger site extended to 6.8 m depth and is the westernmost of the three boreholes on the Finley terrace surface (see Figure 5b for location and Figure 6 for description). At depths 0–3.50 m in the WL borehole, the largest grain size percentage is medium silt. Sediment grain size is relatively uniform from the surface to 3.50 m depth: the clay, very fine silt, and fine silt fractions decrease slightly with depth and the medium silt and coarse silt increase slightly with depth, consistent with dust infiltration and pedogenesis at the modern surface, but otherwise the grain size is consistent and dominated by medium and coarse silt. Sand is absent from 0 to 3.5 m except for the upper 1.5 m, which includes <1.5% disseminated medium and coarse sand.

Below ~3.5 m, the sediment becomes much more heterogeneous in grain size. There is a slight increase in medium sand at 3.50 m and a second small 0.5%–1% spike in medium, coarse, and very coarse sand at 4.00 m. Between 4.00 and 5.80 m depth, grain size percentages are more variable, do not consistently increase or decrease with depth, and the largest grain size percentage is coarse silt. At ~5.80 m depth, the coarser fractions increase, and the largest percentage is fine sand sized. From 6.00–7.00 m, the largest grain size percentage returns to medium and coarse silt with moderate amounts on clay, very fine silt, and fine silt.

We encountered a disturbed layer extending from the surface to ~0.45 m depth that exhibits a browner color than the auger samples below, which we interpret as the modern disturbed layer or depth of plowing. Below the disturbed layer to 3.65 m depth, the sediment has relatively homogenous color accompanying the massive texture. Colors fluctuate and grade below ~3.65 m, with prominent darker brown horizons near 3.65–3.95 m and 5.65–6.00 m that may represent periods of relative surface stability and incipient soil formation.

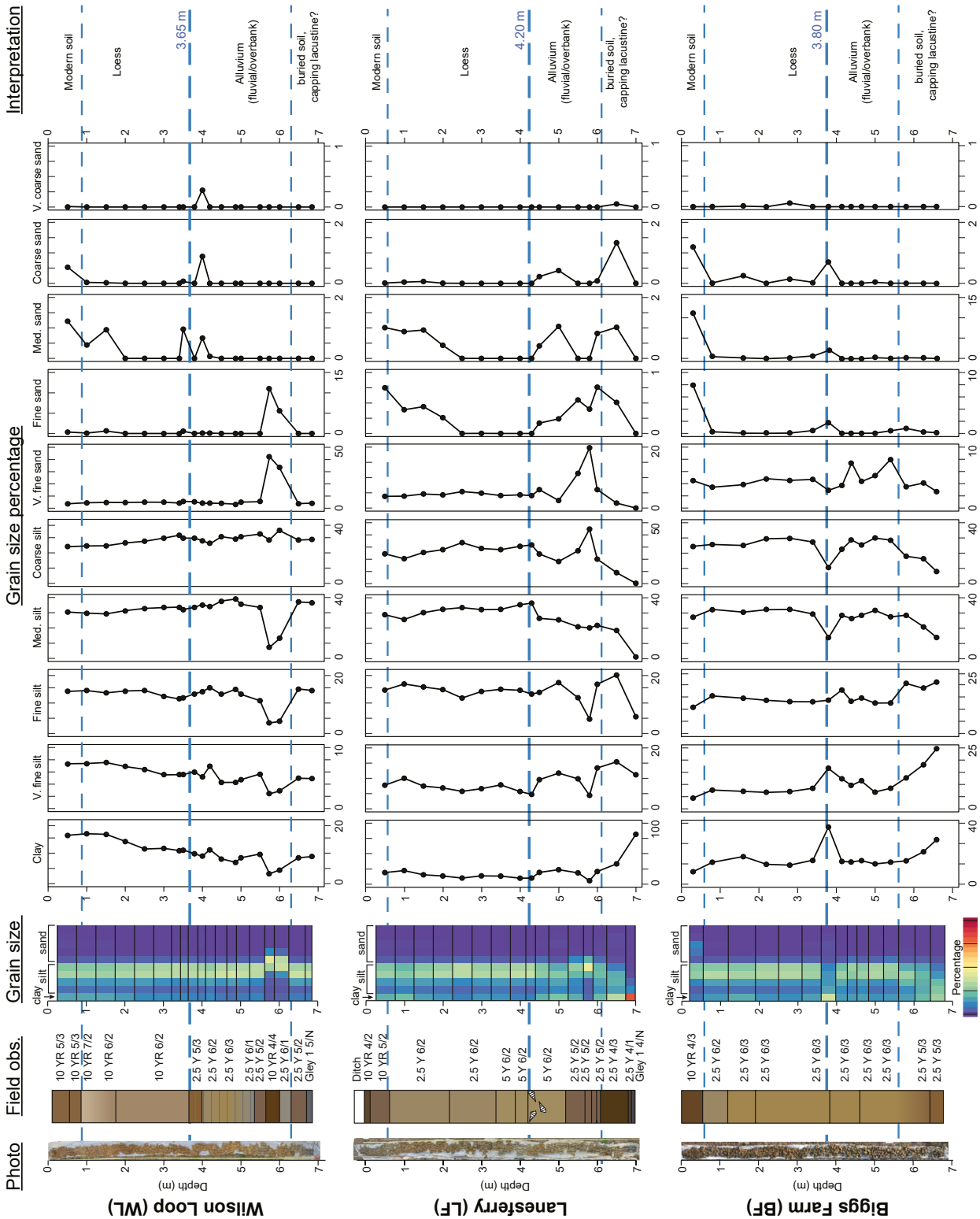

Figure 6. Summary of key hand-soil-auger borehole results from the Finley terrace locations in Figure 5, full results in Delano et al. (2021). Note that horizontal scales vary for each panel to highlight subtle changes in grain size. The "Field Obs." column includes simplified stratigraphic observations such as field-delineated units (black horizontal lines), laminations (gray lines), color changes/gradations, and fossils. Horizontal break lines in the "Grain Size" heat map are midpoints between sample depths. The interpreted transition from loess to alluvium occurs between 3.65 m (Wilson Loop) and 4.20 m (Lanesferry) depth and is marked by a change from homogenous silt to interbedded heterogeneous sand, silt, and clay, and well as the presence of gastropods, laminations, and pronounced color changes due presumably to varying oxidation-reduction conditions. The loess unit has almost no sand below ~1.5 m depth, but notable subtle spikes occur below the interpreted loess/alluvium contact. The base of each auger borehole is marked by a sharp transition to increased fractions of fine to medium silt and/or clay, in some cases gley, which may record paleolakes associated with the horizontal terrace gradient.

From 3.65–5.35 m, weak horizontal banding 1–3 mm thick is pervasive and visible as subtle color changes. Notably, at 6.70–6.85 m depth, the auger sample colors transitioned to gley (anoxic), rather than the varying shades of reddish, grayish, or yellow-brown (oxidized) seen elsewhere in the auger hole. Because this color transition to gleyed is accompanied by a significant clay fraction in borehole LF, we interpret this color change as recording a significant change in depositional setting rather than a modern groundwater signal.

Our preferred interpretation for the location of the loess-alluvium contact at the WL site is at ~3.65 m depth below the terrace tread (Figures 6 and 7) based on the appearance of sand fractions between 3.50 and 4.00 m as well as prominent changes in texture, color, and banding observed in the field. Above ~3.65 m depth in borehole WL, the sediment is remarkably homogenous in grain size and color, whereas below ~3.65 m the borehole exhibits significant variability in texture, color, and banding. Variation in color corresponds to shifts in grain size below ~3.65 m in borehole WL. If the transition from loess to alluvium is interpreted on grain size alone, an alternative contact is near 5.6 m depth, where a significant increase in very fine and fine sand is observed (Figure 6). We think this interpretation is unlikely for reasons that incorporate observations from all three boreholes, listed in section 4.1.1.4 below. We interpret the massive, stiff, silt-dominated material at the bottom of the borehole (6.3–7.0 m) as lacustrine deposits, which is anoxic (gleyed) at depth and oxidized near a paleosurface in which a soil was formed and subsequently buried.

4.1.1.2. Lanesferry Road (LF) Soil Auger Borehole and Subsurface Stratigraphy

The Lanesferry Road (LF) borehole extended to a depth of 7.0 m and was collected from a ditch ~0.3 m below the terrace tread elevation. Similar to the other two boreholes, the grain size distribution is homog-

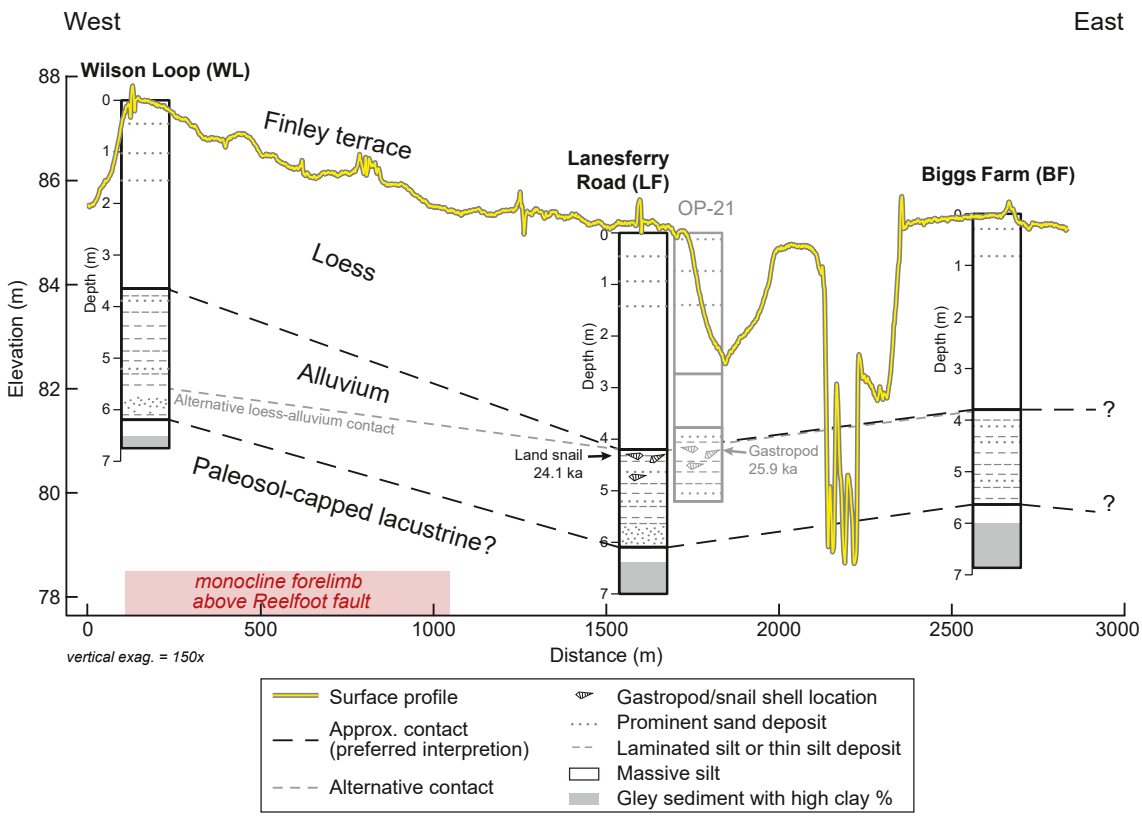

Figure 7. Interpreted simplified stratigraphy from auger profile on the Finley terrace across the Reelfoot fault monocline forelimb (red box) (location in Figure 5). Yellow line is surface elevation profile. We present two possibilities for the loess-alluvium contact based on uncertainty in the Wilson Loop stratigraphy (3.65 m or 5.6 m depth), however, the alluvium-lacustrine contact parallels the higher contact (3.65 m in Wilson Loop, our preferred interpretation). Stratigraphic contacts parallel the surface and appear warped across the fault projection, indicating fault deformation rather than loess thickening to the west. OP-21 is simplified borehole stratigraphy and recalibrated unidentified gastropod age from nearby core reported by Rodbell (1996), projected to the same profile. OP-21 stratigraphy, depth to gastropod fossils, and gastropod radiocarbon ages agree with findings from this study.

Table 1
Radiocarbon Age Results of the Finley Terrace

Sample ID	Location	Material	$F^{14}C$	^{14}C age [yrs BP]	Calibrated age [cal yrs BP]
OB-LF-420-425	−89.35767, 36.17149	Gastropod shell *Pomatiopsis lapidaria*	0.0827 ± 0.0015	20,030 ± 150	24,457–23,782

enous in the topmost ~4.20 m of the borehole, with the highest grain size fraction of medium silt. The upper 2.0 m has a slightly higher (0.5%–2%) concentration of disseminated fine and medium sand than the underlying stratigraphy. The clay fraction decreases gradually with depth and the medium and coarse silt fraction gradually increases with depth until 4.30 m, consistent with dust infiltration and incipient soil formation in the modern surface. From 4.30–6.10 m, grain size percentages fluctuate but generally there are higher percentages of clay, very fine silt, medium silt, and sand fractions than the upper 4.30 m. From 6.10 to 7.0 m, grain sizes generally fine with depth before an abrupt change to dominantly clay at 7.0 m, which prevented further augering.

Below the modern disturbed layer extending to 0.65 m depth, the auger profile color is homogenous light brownish gray and light olive gray with mottled oxidation. The color darkens to grayish brown near ~5.20 m, darkens further to olive brown near 6.10 m and dark gray near 6.70 m, and exhibits gley (anoxic conditions) below 6.80–6.90 m. The color change at 6.10 m coincides with a textural change from (a) variable, fluctuating grain sizes with sporadic laminations and mottled oxidation to (b) stiff, massive silt and clay with no visible texture (such as laminations) and little to no oxidation until the bottom of the borehole.

Between 4.20 and 5.20 m, we observed small gastropod shells with the densest concentration between 4.20 and 4.35 m depth (Figure S1) as well as small white precipitated tubes that are interpreted as burrow casts. These were the only shells observed and the only datable carbon material recovered in any of the three auger holes. The gastropod shells were identified as *Pomatiopsis lapidaria* (Nekola & Pigati, 2018, written communication), a freshwater amphibious (quasi-terrestrial) snail species typically found in flooded riparian forests. The LF site is the closest of our three sites to core OP-21 from Rodbell and Schweig (1993), which was collected from the same Finley terrace surface (Figure 5b). Rodbell and Schweig (1993) noted gastropod shells at 4.07–4.40 m depth in the OP-21 core only, although the species was not identified. Other snail species have previously been identified in this region in the Peoria Loess within the bluffs, which caps the Finley terrace, but these are purely terrestrial snails that live in drier environments rather than the semi-aquatic species found here (Pigati et al., 2015). The presence of *Pomatiopsis lapidaria* suggests that the sediment at ~4.20–5.20 m depth was deposited in a wetter, fluvial environment rather than as loess, which drains very well. As noted above, carbonates appear to be leached above 4.00 m depth, which could prevent snail shell preservation at this site (Snowden & Priddy, 1968). However, because we identified snail shells beginning at 4.20 m depth, and snails were discovered nearby at 4.07 m depth (Rodbell & Schweig, 1993), we interpret the appearance of shells as a stratigraphic contact rather than a carbonate leaching boundary. Notably, the first prominent grain size change occurs slightly below the occurrence of these snail fossils at ~4.30 m rather than at ~4.20 m depth.

The *Pomatiopsis lapidaria* shells (Table 1) yielded a calibrated radiocarbon age of 24,457–23,782 cal yrs BP (95% confidence, median probability 24,052 cal yrs BP). The radiocarbon age from (Rodbell & Schweig 1993; Table 1) is calibrated here to 26,372–25,598 cal yrs BP (95% confidence, median probability 25,905 cal yrs BP). Gastropod shells can yield radiocarbon ages that are slightly too old due to incorporation of old carbon from carbonate rocks or sediment, although the snail taxa previously studied in the Peoria Loess typically incorporate only small amounts of old carbon (1%–5%) (Pigati et al., 2015). While *Pomatiopsis lapidaria* carbon incorporation has not been studied, we assume a similar accuracy to within a few hundred years.

We interpret the most likely depth of the loess/alluvium contact to be ~4.20 m (~4.5 m below terrace tread) (Figures 6 and 7), based on the appearance of floodplain snail species followed by a pronounced shift in grain size distributions from consistently medium silt to 4.20 m depth to more variable grain sizes and ultimately clay 0.1 m below 4.20 m. The presence of the flooded riparian forest snail species *Pomatiopsis lapidaria* adds robustness to the interpreted location of the loess-alluvium contact at the LF site. We identify a transition to fine grain sizes below 6.10 m and interpret this material as a lacustrine deposit, which is oxidized closer to the paleosurface and not oxidized at depth (gley) (Figures 6 and 7).

4.1.1.3. Biggs Farm (BF) Soil Auger Borehole and Subsurface Stratigraphy

The BF borehole extended to 6.8 m depth and is the easternmost of the three boreholes. The shallow sediment recovered from the BF borehole (0–0.3 m) shows the highest percentage of sand found at any depth of the three auger sites (11% medium sand at 0.30 m). We interpret this sand as late-stage flood deposits on the Finley surface, presumably after most of the surface had been abandoned and covered with eolian silt. This sand may have originated from the nearby Biffle Creek, a tributary to the Obion River (Figure 5a), or possibly from nearshore reworking of Obion Lake recorded by Crockett (1834) and Lyell (1849), (described further in section 5. Historical Data) although the extent of that lake is uncertain and no clear diagnostic bedforms could be recovered from the auger. Rodbell (1996) also noted relatively high percentages in sand near the surface at nearby core OP-21 (Figure 5) which was attributed to possible coseismic sandblows. Between 0.30 and 3.80 m depth, the largest grain size percentage is medium silt with moderate clay and fine silt but virtually no sand (Figure 6). The coarse silt and very fine sand fraction gradually increase with depth while the clay, very fine silt, and fine silt gradually decreases with depth over this section, consistent with other auger sites. At 3.80 m depth is a lens with high concentrations (~40%) of clay. Below 3.80 m depth, the grain size fractions fluctuate, but on average, grain size decreases from 3.8 m to the bottom of the borehole at 6.8 m. The lowest sample at 6.60 m is dominated by clay (Figure 6).

Sediment collected from the BF borehole was examined in low-light conditions; therefore, observations of color were more uncertain and apparently more uniform at this site than the other two auger sites. We repeated Munsell color observations upon returning from the field within two days, but the colors reported here may represent some oxidation that occurred in the days following sample collection.

The topmost layer (to 0.55 m depth) is disturbed, likely from plowing, and is olive brown (Figure 6). Below the disturbed layer, recovered sediment becomes mottled and lightens to light brownish gray (0.55–1.20 m). This layer displays intermittent sand lenses associated with the mottled sediment that is lighter in color than the average unit color. At greater depths, the sediment color is typically light yellowish brown (1.2–6.25 m) and darkens slightly to light olive brown near the base of the borehole (6.25–6.80 m) (Figure 6). Importantly, we noted a slight soil textural change near 3.85 m depth that coincided with a change in oxidation mottling in the field (Table S7) in the companion data repository (Delano et al., 2021). Auger sample texture is fairly homogenous and massive from 1.20–4.63 m but shows intermittent liquefied sand lenses below 4.63 m.

We interpret the loess/alluvium contact of the BF borehole at ~3.80 m depth (Figures 6 and 7), which coincides with a sharp increase of clay, very fine silt, and sand fractions, a decrease in silt-sized grains, and marks the top of a sequence where grain sizes fluctuate. This depth approximately coincides with a field-identified change in texture and prevalence in oxidation mottling at 3.85 m (within auger depth uncertainty). We interpret a relatively abrupt grain size fining trend near ~5.6 m as a possible contact between alluvium and soil-capped lacustrine deposits, although the contact may be gradational (Figures 6 and 7).

4.1.1.4. Alternative Interpretation of Loess-Alluvium Contact

Here, we explore the alternative interpretation that the loess-alluvium contact is deeper in either or both the WL and LF boreholes based on the observed shift to a relatively coarser grain size (from medium-silt dominated above to very fine sand dominated below). This scenario implies the loess-alluvium contact across the auger transect occurs at ~5.6 m (WL borehole), ~5.8 m (LF borehole), and ~3.8 m (BF borehole) below the terrace surface from west to east. However, this interpretation requires that we ignore other indicators of depositional environment such as color, texture, and the presence or absence of *P. lapidaria* fossils. Several observations are at odds with the interpretation that the loess-alluvium contact is deeper. First, in the LF borehole, this coarser horizon is clearly below the appearance of the flooded riparian forest snail species *P. lapidaria*. We find the appearance of *P. lapidaria* compelling evidence of the abrupt environmental change at 4.2 m depth in the LF borehole accompanying the loess-alluvium transition. Second, we observe a prominent anoxic gleyed silty clay or stiff silt near 7 m depth in all boreholes. These silty clays and stiff silt most likely record a lacustrine setting, but the reinterpretation that the loess-alluvium contact is at ~5.6 m in the WL borehole but at 4.2 m in the LF borehole—if we accept that *P. lapidaria* marks the loess-alluvium contact—would require significant thickening of the alluvium upstream from borehole WL (Figure 7).

Finally, sediment in the uppermost ~3.8–4.2 m of each borehole is remarkably uniform, whereas below these depths significant color and textural variation exists in all boreholes, indicating a pronounced shift in depositional environments, which also corresponds with the occurrence of *P. lapidaria* in the LF borehole. With all these factors in mind, we attribute the subtle grain size changes at the loess-alluvium contact in the WL borehole (and other boreholes) to the high proportion of reworked loess in the drainage, similar to previous findings (Rodbell, 1996).

4.1.2. Holocene Floodplain (Qa)

The Holocene floodplain (Qa) is consistently 2–4 m above the modern channel (Figure 4). Although the surface has been anthropogenically modified, evidence of abandoned oxbow lakes and well-preserved meandering channel morphology is widespread. The Holocene floodplain widens upstream from 0.5 – 1.3 km wide near the bluff margin (between 1 to 2 km valley distance) to 3.0–3.3 km wide at valley distances 18 to 33 km (Figure 3). The Holocene floodplain gradient is approximately zero from valley distances 0 to 5 km and parallels the modern channel gradient at distances >5 km (Figure 4).

4.1.3. Deweyville Complex Terraces (Qtda and Qtdb)

The Deweyville complex terraces (Qtda and Qtdb) are newly mapped in the Obion River valley and are interpreted as correlative to terraces observed elsewhere in the Mississippi Embayment (Autin et al., 1991; Saucier & Fleetwood, 1970). Where mapped outside the Obion River valley, the Deweyville complex occurs between the Holocene floodplain and Prairie complex (temporally equivalent to Finley and Hatchie terraces). The Deweyville complex elsewhere is characterized by well-preserved, oversized channel migration features compared to Holocene contemporaries and frequently is buried by Holocene deposits at lower elevations (Autin et al., 1991; Saucier & Fleetwood, 1970). These characteristics are consistent with our observations—in the Obion River valley, Deweyville complex terraces are inset below the Finley terrace, nearly merge with the Holocene floodplain, and in some instances preserve migrating channel morphology (e.g., point-bar accretion meander scrolls or scroll bars) that are oversized compared to the modern Obion River channel (Saucier, 1987) (Figure 5). We subdivide the Deweyville complex terraces in the Obion River valley based on relative position and use Deweyville A (Qtda) for the slightly higher elevation, apparently older terraces and Deweyville B (Qtdb) for the slightly lower elevation, younger terraces. The Deweyville complex terrace treads are typically 1–3 m above and smoother than the Holocene floodplain (Figure 4). The Deweyville complex terraces are only present in the lower Obion River valley; at ~13 km valley distance, they merge with the Finley terrace tread elevations (Figure 4). The longitudinal valley profiles suggest the Deweyville complex terraces may reflect incision from the Finley terrace profile following a base level decrease, consistent with other mapped locations, implying that the highest Deweyville complex terrace surfaces may be nearly contemporaneous with (but slightly postdate) the latest Finley terrace deposition (Autin et al., 1991) (Figure 4). The oversized preserved meander scrolls noted by Saucier (1987) indicate deposition when the paleo-Obion River had a different flow rate, annual discharge, or vegetation cover than the modern Obion River (Autin et al., 1991). The crisp expression of these original, oversized meander scrolls suggests that post-depositional surface modification (e.g., recent flood deposits, loess accumulation) on the Deweyville complex terraces is minor. Coring data presented in Van Arsdale (1999) on the Deweyville A surface (mapped there as floodplain) do not indicate a loess cap. Limited loess on the Deweyville complex suggests that the terrace deposition postdates the most recent loess deposit, the Peoria Loess, which may be as young as 10–11 ka (Gold et al., 2019; McKay, 1979; Ruhe, 1983).

4.1.4. Hatchie Terrace (Qtha)

The Hatchie terrace (Qtha) is the most continuous terrace within the mapping extent and primarily occurs on the northern side of the valley as a single, continuous, somewhat dissected terrace tread (Figure 3). The relative height of the Hatchie terrace above the Holocene floodplain (Qa) ranges from 15 to 29 m near the valley mouth (valley distance 0 to 3 km) and gradually decreases upstream to ~3 m above Qa near ~30 km valley distance (Figure 4). Valley longitudinal profiles reveal a moderate reverse gradient of 3.5 m/km (0.20°) to the northeast at between 0 and 3 km valley distance (Figure 5), a slight reverse gradient of 0.4 m/km (0.02°) from 3 to 15 km valley distance, and a near-zero gradient at distances >15 km (Figure 4).

We map the westernmost terrace tread in the Obion River valley (location A in Figures 3b and 5b) as the Hatchie terrace. Our interpretation differs from that of Saucier (1987). The abrupt reverse gradient on the western terrace edge, described as a terrace "lip" (Saucier, 1987), was interpreted previously as either (a) a remnant of an older, higher terrace that grades into the Hatchie terrace to the east (Saucier, 1987), (b) a continuation of the Hatchie terrace, which contains westward-thickening loess (Rodbell, 1996), or (c) a continuation of the Hatchie terrace that has been uplifted by the Reelfoot fault (Van Arsdale et al., 1999). We interpret this surface as a continuation of the Hatchie terrace observed upstream for the following reasons: the tread is uniformly incised, and the transitional slope is relatively gentle, with no obvious riser to indicate a contact between older and younger terraces as seen elsewhere in the valley.

4.1.5. Humboldt (Qthu) and Henderson (Qthe) Terraces

Terrace identification, correlation, and differentiation from the surrounding bluffs is more difficult for surfaces older than the Hatchie terrace due to the thick loess cover and a high degree of dissection. Here again, our terrace mapping diverges from previous studies (Rodbell, 1996; Saucier, 1987). The Humboldt terrace (Qthu) is the second-oldest identified terrace and is only identified in the upstream extents of the Obion River valley (>15 km valley distance) and does not cross the Reelfoot fault monocline trace (Figure 3). The tread is moderately to heavily dissected and resides ~15 m above the modern floodplain (Figure 4). The preserved Humboldt terrace surfaces have a gradient that roughly parallels the Holocene floodplain and modern channel (~0.3 m/km [0.02°] to the southwest), although scatter in elevations derived from the dissected loess-covered surface makes the true terrace tread gradient difficult to determine (Figure 4).

The Henderson terrace (Qthe), which was previously not mapped in the Obion River valley, is heavily dissected and typically lacks clear indication of a once-planar tread that is visible in the younger surfaces (Figure 3). Some of the Henderson terraces identified in this study were previously mapped as Humboldt terrace surfaces (Rodbell, 1996). Differing interpretations here are based on large elevation differences and increased degree of incision between Humboldt terraces mapped by Saucier (1987). These subtle surficial changes are more easily resolved in the high-resolution, lidar-derived DEMs than in the original topographic maps used by Rodbell (1996) and Saucier (1987). The Henderson terrace is identified primarily based on elevation and comparing the surface texture to the surrounding bluffs—the Henderson terrace is generally smoother, with overall flatter terrain than the bluffs. Additionally, the contact of the Henderson terrace with the bluffs is typically marked by a steep scarp or slope increase indicative of an inset surface. Due to the degraded condition, the depiction of the Henderson terrace is uncertain (Figure 4). Overall, the Henderson terrace gradient (~0.45 m/km [0.025°] to the southwest) is slightly steeper than the Holocene floodplain for all but the lower 5 km valley distance, but elevation points have significant scatter likely due to variation in post-depositional loess cover and erosion (Figure 4). The westernmost Henderson terrace tread, closest to the Reelfoot monocline trace, may indicate a reverse gradient as with the younger terrace surfaces (Figure 4). However, the unknown amount of post-depositional loess cover and incision complicates identification of the original tread and could influence the apparent gradient.

4.2. Shorelines

We map a series of apparent shoreline features, previously identified by Saucier (1987) in the Obion River valley and with additional mapping here. The shoreline landforms manifest as approximately valley-parallel, symmetrical, elongated ridges that we interpret as constructional lacustrine beach ridges (Figure 3). Often, these ridges are nested as a series of similar-elevation complexes or decrease in elevation away from the bluff margin. Most beach ridge complexes are concentrated near the confluence of smaller tributaries with the main Obion River valley or along the outer margin of a terrace tread, although some ridges appear isolated on the terrace tread near the riser. We separate these ridge complexes into three groups (beach ridges 3, 2, and 1; Figure 3b) based on elevation, lateral ridge continuity, and apparent preservation. We extracted elevation points at the highest point of the best-preserved ridge crests to compare to the terrace longitudinal profiles. The beach ridge units have not been excavated in previous studies or this investigation, and interpretations are based on morphology from the lidar only.

4.2.1. Beach Ridge 1 (Qbr1)

Beach ridge 1 (Qbr1) is the highest ridge complex and is typically 95–97 m in elevation (Figure 4). Beach ridge 1 only appears between 15 and 35 km valley distance and is the most eroded, with smoother peaks and discontinuous ridges (Figure 4). The bluff-proximal contact of beach ridge 1 appears to be inset into the Henderson terrace, which suggests beach ridge 1 formed after the Henderson terrace; however, the relationship with the Humboldt and Hatchie terraces is unclear.

4.2.2. Beach Ridge 2 (Qbr2)

Beach ridge 2 (Qbr2) has the widest distribution and has ridge elevations of 88–92 m at valley distances >10 km and 92–95 m at valley distances <10 km, mimicking the longitudinal profile of the Hatchie terrace tread (Figure 4). Beach ridge 2 crests are typically well defined with relatively sharp peaks that are less incised than beach ridge 1 but show some evidence of post-depositional erosion, which likely contributes to the scatter in elevations. The base of beach ridge 2 is in contact with both the Hatchie and Finley terrace treads, which suggests that beach ridge formation may be decoupled with terrace formation and the associated lake postdates both terraces. At the eastern mapping extent, beach ridge 2 crests are less defined, exhibit less relief above the Hatchie terrace tread, and have been partially buried by tributary alluviation.

4.2.3. Beach Ridge 3 (Qbr3)

Beach ridge 3 (Qbr3) is the lowest beach ridge complex. Elevations are typically 85–87 m at valley distances >10 km, 86–99 m at valley distances 4–10 km, and one mapped ridge at 1 km valley distance has elevations of 91–93 m (Figure 4). Beach ridge 3 is only found in contact with the Finley terrace or nested in beach ridge 2, suggesting it postdates both landforms. The ridges typically occur near the outer Finley terrace contact closest to the bluffs, and crests are typically 2–3 m above the Finley tread. The farthest upstream occurrences of beach ridge 3 are patchy, discontinuous, and have low relief (<2 m) above the Finley terrace suggesting partial burial by more recent alluviation. Beach ridge 3 is absent at valley distances >25 km.

4.2.4. Origin of Beach Ridges

There are multiple explanations for lake, beach ridge, and terrace formation in the Obion River valley. One possibility, documented historically (elaborated in "Historical Data" section), is that lakes may form in response to damming of the Obion River due to surface deformation above the Reelfoot fault. It is also possible lakes formed and fluctuated rapidly due to post-glacial sedimentation that blocked Obion River drainage to the Mississippi River (Autin et al., 1991). The more poorly preserved and discontinuous surface expression of beach ridge 1 compared to beach ridges 2 and 3 suggests an older formation age, whereas the surface morphology of beach ridges 2 and 3 are similar, suggesting they could be related to the same recessional sequence. We lack absolute age control to accurately constrain beach ridge formation timing; however, depositional relationships and relative sharpness in morphology suggest that beach ridge 1 postdates the Henderson terrace (35–55 ka), and beach ridges 1 and 2 both postdate Finley terrace formation. Based on the map pattern of the shorelines and the complicated depositional relationship with the terraces, we suspect a complex history of shoreline reoccupation has occurred. From a tectonic perspective, the presence of beach ridges in the Obion River valley is important because they represent shorelines that formed at a uniform elevation, unlike the terrace elevations, which are complicated by eolian cover and changing river gradients.

4.3. Surface Deformation Measurements From Lidar

4.3.1. The Northern Reelfoot Fold Scarp

The northwestern extent of the Reelfoot fold scarp near New Madrid, Missouri, deformed a late Pleistocene (~20–18 ka) (Rittenour et al., 2007) Mississippi floodplain surface and has 1.3–1.7 m of vertical separation with a preferred value of 1.5 m (Figure 2). Approximately 5 km north of this profile, the scarp height tapers to zero at the presumed northern extent of the active Reelfoot fault. In the Kentucky Bend of the Mississippi River, we measure 3.4–3.9 m of vertical separation on a folded late Holocene Mississippi floodplain surface (Holbrook et al., 2006), with a preferred value of 3.9 m (Figure 2). These vertical separation values are

consistent with previous measurements of ~2 and ~4 m of vertical separation, respectively, by Van Arsdale et al. (1995).

The largest vertical separation measured on the Reelfoot fault is located along the southwestern shore of Reelfoot Lake, where the subaerial side of the monocline was matched with sublacustrine bathymetric data (Carlson & Guccione, 2010). The total vertical separation here is ~11.3 m (Figure 2), which records at least two earthquakes offsetting a late Holocene Mississippi alluvial surface. The single event maximum vertical displacement from the 1812 earthquake at this site is estimated at 5.9 to 8.2 m (Carlson & Guccione, 2010).

4.3.2. The Southern Reelfoot Fold Scarp

The most prominent terrace backtilting occurs on the Deweyville, Finley, and Hatchie terraces near 3 km valley distance (Figures 4 and 5). The western (downstream) margins of the Deweyville, Finley, and Hatchie terraces have been partially eroded from lateral migration of the Mississippi River (Figure 5b). If the terrace treads once returned to the gradient observed upstream, as expected for a broad fold scarp or monocline, this correlative surface no longer exists and cannot be used as a displacement marker. Because correlative surfaces are not available to measure vertical separation in the far field, we can only measure the vertical deviation of the eroded terraces at the mouth of the Obion River with respect to projection of the upstream gradient (Figure 5b). We project the mean gradient from the least-disturbed topography on the eastern side of the profile, which approximates the original surface, to the western edge of the fold and measure the vertical difference. This process is repeated several times (as explained in the Methods) to capture a range of plausible correlative surfaces. For shorthand, we refer to these values as apparent vertical separation; these values are minima due to erosion of the terraces from the Mississippi River.

The following vertical separation results are derived from profiles along the least-modified or incised swaths of the Deweyville, Finley, and Hatchie terraces. The minimum apparent vertical separation inferred from the warped terraces is 1.1 m for the Deweyville A terrace (range 0.9–1.1 m), 2.4 m for the Finley terrace (range 2.0–2.6 m), and 8.1 m for the Hatchie terrace (range 7.7–8.1 m) (Figure 5b). The pattern of apparent vertical separation is consistent with progressive deformation of increasingly older surfaces. We also measure the gradient of the apparently tilted terrace treads, using negative values to indicate drainage direction up valley (northeast). Upstream of the surface projection of the Reelfoot fault, the Deweyville, Finley, and Hatchie terraces are nearly horizontal to slightly reverse (Figures 4 and 5b). Downstream from the Reelfoot fault projected trace, the terrace gradients are −1.1 m/km for the Deweyville terrace, −1.4 m/km on the Finley terrace, and −3.5 m/km on the Hatchie terrace (Figure 5). Similar to the pattern of apparent vertical separation, reverse terrace gradients progressively increase with terrace age.

4.3.3. Other Possible Tectonic Features

Other geomorphic features in the Obion River valley could also indicate tectonic deformation but are less reliable. Van Arsdale et al. (1999) first noted that the Obion River floodplain constricts near the projected Reelfoot fault trace. At the mouth of the Obion River valley and near the surface projection of the Reelfoot fault, the Holocene floodplain width is 0.5 km (excluding the Deweyville terraces). If the definition of the Holocene floodplain is expanded to include the Deweyville terraces, the floodplain is up to 1.5 km wide at valley distances <5 km, compared to 3–3.3 km wide farther upstream (Figure 3). Van Arsdale (1999) and Rodbell (1996) observed a reverse Holocene floodplain gradient near the Reelfoot fault; however, these profiles lump the Deweyville terraces with the floodplain and are highly generalized. Our measured gradient of approximately zero on the Holocene floodplain could either reflect Mississippi backwater flooding and sedimentation or a tectonic influence, or both.

Longitudinal valley profiles provide some additional possible insight into tectonic warping after the beach ridges formed (Figure 4). Beach ridges 2 and 3 are horizontal within uncertainty at valley distances >10 km and apparently rise slightly in elevation downstream at valley distances <10 km (Figure 4). Beach ridge 3 may record a more substantial elevation increase near the valley mouth, although the record is very sparse (Figure 4). These correspond to an apparent vertical separation of 2–3 m, or up to ~5 m for beach ridge 3, although no single ridge is large enough to continuously record deformation across the width of the fold

scarp. Since shorelines form horizontally, we interpret the tilting of the profiles of beach ridges 2 and 3 as tectonic.

A final qualitative indicator of terrace deformation, visible in the lidar DEM, is that the incision patterns on the westernmost Hatchie terrace indicate long-lived drainage up valley (to the east), opposite the Obion River valley drainage direction (Figure 5). This drainage pattern could reflect uplift above the projection of the Reelfoot fault, potentially accentuated by a wedge of westward-thickening loess. However, we cannot distinguish drainage direction as influenced by tectonic deformation versus non-tectonic processes, such as diversion caused by sedimentation from the Mississippi River valley.

5. Historical Data

Several historical records document evidence of a lake in the Obion River valley. Van Arsdale et al. (1999) first noted a lake existed in the Obion River valley as early as 1832 (Rhea, 1832) and speculated that this lake had a tectonic origin. However, explicit historical evidence linking the lake to the earthquake sequence of 1811–1812 had remained elusive.

We find additional historical evidence of a lake in the Obion River valley at least as early as 1825 in an autobiography with dated passages. During a bear hunt in the fall of 1825, Davy (Crockett, 1834, pp. 108, 114) describes his destination as, "*started to take a hunt between the Obion lake and the Red-foot lake*," further describing that "*The woods were very rough and hilly*."

The "hilly" terrain between the two lakes is consistent with the bluffs between the Obion River valley and Reelfoot Lake (Figure 2). The historical map of Russell (1795) shows the modern Reelfoot River, the drainage that was dammed to create Reelfoot Lake during the 1812 earthquake, depicted as the "Red-foot River." This may be a colloquial name that persisted locally through to Crockett's time.

The presence of a lake postdating 1812 does not necessarily indicate coseismic formation, given the prevalence of backwater flooding in the Obion River valley from the Mississippi River (Shankman & Samson, 1991). However, (Lyell, 1849, p. 180) recorded, "*The sunk country is not confined to the region west of the Mississippi; for, on my way up the river, I learnt from Mr. Fletcher, a farmer, who had a wooding station in Tennessee, that several extensive forest tracts in that state were submerged during the shocks of 1811–12, and have ever since formed lakes and swamps, among which are those called Obion and Reelfoot.*"

The secondhand report by Lyell strongly suggests that the Obion River was dammed by vertical surface deformation along the Reelfoot fault similar to the Reelfoot River (and subsequent Reelfoot Lake), creating Obion Lake in 1812. A small change in base level near the mouth of the Obion River valley would have a similar effect of lake formation until the stable river gradient reestablished. The lake referenced by Lyell (1849) may be the same lake depicted by Rhea (1832) and mentioned by Crockett in 1825 (Crockett, 1834). Reelfoot Lake may have outlasted Obion Lake into modern times because it occupied depressions from old Mississippi River meander bends (Fuller, 1912; Russ, 1982), has a high water table (Carlson & Guccione, 2010), and was later anthropogenically regulated with a spillway (U.S. Department of the Interior Fish and Wildlife Service, 1989), while the Obion River would eventually breach the natural dam caused by the Reelfoot fold scarp, allowing the lake to drain. Fold scarp heights in the Obion valley are also smaller (1–2 m; Figure 5) than scarps bounding Reelfoot Lake (6–8 m in 1812; Figure 2) (Carlson & Guccione, 2010), and consequently easier to breach.

6. Discussion

6.1. Blind Faulting

Recent motion on blind reverse faults can be challenging to detect and quantify because deep fault slip does not break the surface along readily recognized scarps. Broad, distributed folding of late Quaternary surfaces and warped and deformed terraces are often the only tectonic signature of blind faults (e.g., Bullard & Lettis, 1993). High-resolution topography, especially bare-earth models derived from lidar, are particularly useful for deciphering subtle signals of landscape deformation from blind faults (e.g., Meigs, 2013; Thomp-

son Jobe et al., 2020), and these data are especially important in highly vegetated, subtropical, and active landscapes such as the Mississippi Embayment. With these new data, we evaluate whether apparently warped landforms in the lower Obion River valley record evidence of tectonic deformation, climate-driven processes, or a combination of both. The landforms studied here contain influences of backwater flooding, changes in base level, and potentially fluctuating lake levels. However, our surficial observations from lidar, subsurface borehole data, and historical accounts of lake formation are also consistent with blind faulting along the Reelfoot fault since the late Pleistocene and potentially in older, late Quaternary surfaces. Disentangling these two signals is challenging but merits investigation and is elaborated below.

6.2. Surface Deformation in the Obion River Valley

Three lines of evidence favor the interpretation that surface folding due to buried faulting is preserved in the landscape at the confluence of the Obion and Mississippi River valleys: (a) increased tilting of progressively older terrace surfaces; (b) the constant thickness of loess on the Finley terrace surface as determined from boreholes; and (c) apparent deformation of previously horizontal shorelines. These geomorphic observations, along with historical records of lake formation following the 1812 earthquake and valley constriction near the Obion River valley mouth, are consistent with uplift above the southern extent of the Reelfoot fault.

6.2.1. Deformed Terraces

We document progressive deformation of the Deweyville A, Finley, and Hatchie terraces that suggests repeated earthquakes along the southern extent of the Reelfoot fault. At the scale of the entire valley, there appears to be two hingelines where terrace gradient values decrease downvalley: a prominent hinge at ~3 km valley distance seen in the Deweyville, Finley, Hatchie and possibly Humboldt terraces and a subtle hinge at ~12 km distance seen in the Finley and Hatchie terraces (Figure 4). Importantly, the terraces that record the subtle hingeline at ~12 km (Finley and Hatchie) also preserve lacustrine landforms, such as horizontal gradients and beach ridges. Therefore, the subtle gradient hinge at ~12 km valley distance may reflect lacustrine or backwater flood influence, such as short-lived upstream deposition from the Mississippi River overbank flow. Alternatively, apparent backtilting between 3 and 12 km valley distance on the Finley and Hatchie terraces may reflect small, meter-scale variation in tread preservation across the valley length since deposition in the late Pleistocene.

The most apparent folding on these three terraces (~3 km valley distance in the Obion River valley) occurs along a linear trend and coincides with the eastward cessation of modern seismicity (Figures 2 and 3), consistent with buried fault tip near that location. Reverse gradients from 0 to 3 km valley distance are steeper than the modern or prehistoric river gradients preserved upstream, suggesting a non-fluvial origin rather than backwater flooding. Specific evidence for progressive deformation includes increased reverse surface gradient as a function of increasing terrace age and an associated increase in the minimum apparent vertical separation. These observations suggest that older terraces record more tectonic deformation and therefore a longer earthquake record than younger terraces. Assuming all observed tilting is due to tectonic deformation, progressive folding across the three terraces implies earthquake events between deposition of the Hatchie terrace and the Finley terrace (~35–55 ka to 24 ka) (Leigh & Knox, 1993; Rodbell, 1996; Rodbell et al., 1997), between deposition of the Finley and Deweyville terrace (<24 ka), and postdating Deweyville terrace deposition. We cannot, however, estimate the number of events, exact event timing, or slip amount per event.

6.2.2. Loess Thickness From the Auger Profile

Three auger boreholes along a 2.6-km-long transect spanning a prominent hingeline of backtilting on the Finley terrace reveal a coherent package of warped loess, alluvium, and lacustrine deposits (Figure 7). Across all three boreholes, our interpreted contact between loess and alluvium occurs at 3.7–4.5 m below the terrace tread and mirrors the surface profile (Figure 7); therefore, a wedge of decreasing loess thickness extending west to east does not appear to explain ~2 m of surface warping over the same distance. Instead, the loess-alluvium contact similarly shows ~2 m of vertical separation, although fewer profile elevations are available due to the limited auger sites compared to elevations extracted from the lidar. This pattern is mirrored with an interpreted lacustrine deposit ~7 m below the surface at all sites (Figures 6 and 7), which

likely formed at a uniform elevation. We interpret the consistency between warping of the surface and two subsurface contacts as evidence of broad folding related to buried slip on the Reelfoot fault.

Our stratigraphic results from the Finley terrace are consistent with findings from previous studies. The 4.20 m depth to snail fossils in our LF borehole is consistent with the unidentified gastropod fossils found by Rodbell (1996) in OP-21 at 4.07 m (Figure 7). Previous work by Van Arsdale et al. (1999) provides generalized stratigraphic context from cores extracted prior to Obion River channelization that parallel our Deweyville A profile (Figure 5). They reported patterns of grain size changes that imply the stratigraphic contacts parallel the subtle surface warping at the approximate Reelfoot fault projection (Van Arsdale et al., 1999). Our study provides additional stratigraphic context by focusing on the loess-alluvium contact, which is likely to be less heterogeneous than alluvium stratigraphy.

Although the Obion River has likely flooded the Deweyville surface since deposition, the clear preservation of original oversized scroll bars suggests a lack of loess cover and minimal surface modification since formation of the terrace (Figure 5b). We lack loess thickness constraints or stratigraphic information for the Hatchie terrace and therefore cannot accurately separate differential loess thickness from tectonic deformation on this surface. While, loess has been documented as thinning from west to east in this region over a much larger area (tens of kilometers), the distribution of thicknesses is sparsely constrained, especially on the Obion River terraces (Rodbell, 1996; Rodbell et al., 1997). We do not expect this regional-scale process to be visible in the few-kilometer-long topographic profiles in this study (Figure 5). The results of the auger profile on the Finley terrace show that the effect of loess thickening at this scale is not significant compared to the coseismic folding, and we extrapolate that inference to the Hatchie terrace as well.

The vertical separation values measured across all three folded terraces are minima. Each deformed terrace represents a fragment of a broad fold, where the original uplifted surface has presumably been removed by erosion from the Mississippi River (Figure 5). Without a correlative surface to provide a deformation marker, we cannot calculate true vertical separation and slip or folding rates.

6.2.3. Paleolakes and Shorelines

Geomorphic mapping and historical records indicate that the Obion River valley has been repeatedly occupied by lakes. The most recent Obion Lake likely formed following the 1812 earthquake and is consistent with damming of the Obion River by motion on the Reelfoot fault, or sufficient base level increase, similar to the formation of Reelfoot Lake. Deformation from the 1812 earthquake may still be preserved as the ~1-m-high broad warping on the Deweyville terrace (Figure 5c).

Older paleolakes are recorded by the near-zero gradients of portions of the Finley and Hatchie terraces and the presence of beach ridge complexes. These paleolakes may reflect tectonic damming from deformation across the Reelfoot fault, but also could have formed from backwater flooding due to post-glacial sediment aggradation on the Mississippi River during glacial retreat (Autin et al., 1991), or both. In either case, landforms from these lakes (Finley and Hatchie terrace treads and beach ridges) provide important horizontal reference frames for later deformation. If each beach ridge unit was originally deposited with uniform elevations, the elevated beach ridges downstream of the Reelfoot fault monocline suggest that the beach ridges have been uplifted by motion on the Reelfoot fault. Additionally, beach ridge profiles parallel the other warped terraces, which could suggest a similar long-term history of folding.

While the Obion Lake shorelines features are mapped using several criteria, such as morphology and inset relationships, several assumptions are inherent in the interpretation that the shorelines record vertical deformation. First, our mapping is based solely on lidar-based imagery and does not include any absolute age control, field mapping, or stratigraphic data to test correlations. Second, the ridges are not widely or consistently preserved along the length of the Obion River valley and are especially scarce near the Reelfoot fault monocline, leading to ambiguity in deformation measurements. Finally, the lack of continuous preservation leads to uncertainty in correlating beach ridge complexes over significant distances. An alternative interpretation to tectonic deformation is that beach ridges that appear west and east the Reelfoot monocline scarp are from different lake levels. If multiple lakes formed rapidly or lake levels fluctuated in short period of time, the differences in age would be nearly indistinguishable without precise age control. In general, since the beach ridge elevations parallel the Finley and Hatchie terraces even where the expressions are

sparse, our preferred interpretation is that tilting of originally horizontal shorelines records tectonic deformation near a blind fault.

6.3. Implications for Fault Tip Depth

Vertical separation of correlative surfaces above the Reelfoot fault is highest near Reelfoot Lake, the approximate center of the fault, and decreases to the north and south (Figures 2 and 5). The northern half of the Reelfoot fault exhibits more discrete folding at the surface, with deformation over a few hundred meters (Figure 2), compared to the broad, ~2-km-wide fold within the Obion River valley (Figure 5). Vertical separation near the northern Reelfoot fault monocline (1.5 m near New Madrid, Figure 2) in 20–18 ka deposits (Rittenour et al., 2007) is similar to the 1.1 and 2.4 m of apparent vertical separation observed in ≤24 ka Deweyville and Finley terraces near the southern fault extent (Figure 5). These values may suggest that terraces in the Obion River valley have experienced a similar earthquake history to the Mississippi River valley surfaces.

Previous work by Champion et al. (2001) on the Reelfoot fault suggests that changes in deformation character along strike indicates a change in active fault tip depth. Their trishear modeling, constrained by folding at depth, estimates that the active fault tip is twice as deep below the southern section of the fault (~1,020 m deep) than along the northern section (~470 m deep), which generates a broader monocline (Champion et al., 2001). The predicted effects of a deeper active fault are consistent with the broader surface folding shown in this study along the southern section of the Reelfoot fault compared to folding in the north (Figure 8). This may also suggest that the Reelfoot fault extends south beyond the Obion River valley along seismicity trends to nearly Dyersburg, Tennessee (Figure 2), but lacks any identifiable surficial expression.

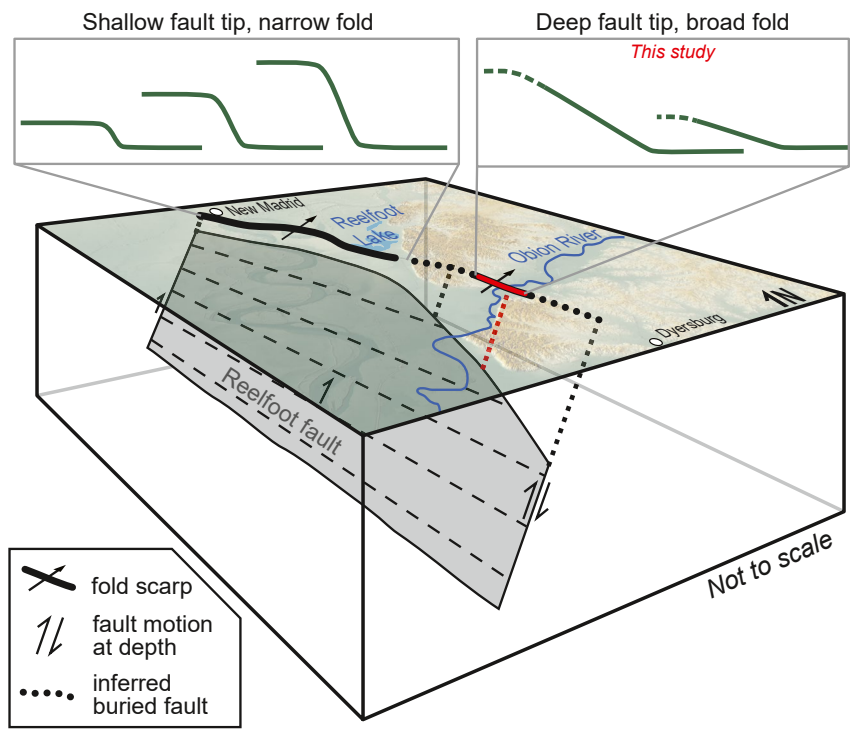

Figure 8. Schematic block diagram (not to scale) of the Reelfoot fault at depth demonstrating how changes in fault tip depth affect the surface expression of deformation (black arrows = sense of slip). The active fault tip is closer to the surface along the northern reaches of the Reelfoot fault and plunges deeper along the southern extent (~470 m deep north of Reelfoot Lake, ~1,020 m deep in the northern Obion River valley) (Champion et al., 2001). As the active fault tip plunges deeper, folding at the surface widens, making surface deformation more difficult to recognize and measure. Fold scarps reach maximum amplitudes near the center of the fault trace by Reelfoot Lake and taper near the margins. Subtle folding is undetectable in the bluffs between valleys due to the dissected topography, which lacks a uniform surface to record deformation.

6.4. Implications for Rupture Length

The historical record of coseismic lake formation and the geomorphic evidence for surface deformation in the Obion River valley suggest that the 1812 earthquake rupture spanned from near New Madrid, Missouri, to at least the Obion River. This rupture length was speculated by Van Arsdale et al. (1999), but conclusive evidence for an 1812 scarp southeast of Reelfoot Lake had not been previously recognized. By combining the northernmost recognized rupture extent (Baldwin et al., 2005; Van Arsdale et al., 1995) with coseismic Obion Lake evidence (Crockett, 1834; Lyell, 1849; Rhea, 1832), the minimum 1812 rupture length is ~58 km. Given the subtle expression of surface deformation in the Obion River valley and evidence for coseismic sackungen that extend nearly to Dyersberg, Tennessee (Delano et al., 2018), the rupture could have extended farther south of Obion River below the bluffs without preserving tectonic surface deformation. This scenario yields a rupture length of ~70 km (Figure 8). Both the 58 and 70 km estimates significantly exceed the previous 1812 rupture length estimate of 32 km (Van Arsdale et al., 1999). Longer rupture lengths lend themselves to larger earthquake magnitudes and are consistent with recent findings that the Reelfoot fault is continuous across the intersection with the Cottonwood Grove and Ridgely faults (Figure 1) (Greenwood et al., 2016).

6.5. Pre-Holocene Movement of the Reelfoot Fault

The progressive deformation recorded in fluvial terraces suggests that the 1812 earthquake on the Reelfoot fault was not the first earthquake to produce surface deformation in the Obion River valley. The surfaces of the Deweyville, Finley, and Hatchie terraces formed <24 ka, ~24 ka, and 35–55 ka (Leigh & Knox, 1993; Rodbell, 1996; Rodbell et al., 1997) and have minimum vertical separations of 1.1, 2.4, and 8.1 m, respectively (Figure 5). These older, deformed terraces likely indicate slow rates of persistent blind slip on the southern section of the Reelfoot fault postdating at least deposition of the Finley terrace and possibly postdating Hatchie terrace deposition. The Finley terrace age (24 ka) and the approximate age of the Hatchie terrace (35–55 ka) yield minimum vertical deformation rates (using apparent vertical separation; see definition above) of 0.1 and 0.1–0.3 mm/yr, respectively. Deformation rates of the Deweyville terrace are based on the observations that the Deweyville terrace surface postdates Peoria Loess deposition (e.g., preserved scroll bars, coring data presented in Van Arsdale et al., [1999]). Using the latest Peoria Loess age of 11 ka (Gold et al., 2019), the minimum apparent vertical deformation rate on the Deweyville terrace is ~0.1 mm/yr. Paleoseismic records on the Reelfoot fault previously recognized earthquakes as early as ~4 ka (Gold et al., 2019); therefore, this study significantly lengthens the paleoseismic record of fault slip on the southern section of the Reelfoot fault.

Other investigators have speculated that activity along the southern section of the Reelfoot fault initiated with the 1812 event (Csontos & Van Arsdale, 2008), caused by a transition of stress from the southeastern rift margin in the Holocene (Cox et al., 2006). By contrast, our study suggests that pre-1812 slip extends along the southern section of the Reelfoot fault, although apparently as buried slip, and has repeated over more than one earthquake cycle during the late Quaternary.

A history of repeated earthquakes extending southeast of the bluff margin is consistent with recent identification and documentation of coseismic sackungen on bluff ridge tops (Figure 2) (Delano et al., 2018; Gold et al., 2019). Gold et al. (2019) demonstrated that these features record at least four earthquakes since 11 ka, including the 1812 event. Delano et al. (2018) suggested that increased shear strain and near-fault deformation may control sackung formation and reactivation. Their mapped distribution of sackungen coincides with the total Reelfoot fault length revealed by modern seismicity, extending south of the Obion River valley. The broad deformation seen in the Obion River terraces likely continues within the bluffs north and south of the river and may contribute to the location of observed coseismic sackungen (Delano et al., 2018); however, the subtle, broad expression would be masked by the thick loess cover and incised topography compared to the relatively smooth and planar terrace surfaces.

6.6. Implications for Current Hazard Models

A key component in seismic hazard models is the length and location of the mapped fault trace (Petersen et al., 2014; U.S. Dept. of Energy, Electric Power Research Institute, and U.S. Nuclear Regulatory Commis-

sion, 2012). The current fault-based source model maps the Reelfoot fault with two geometries: (a) a shorter, 46-km-long segment and (b) a longer, 83-km-long fault that extends farther south and is composed of 56 km of rupture on the Reelfoot fault and 27 km of rupture along the New Madrid West fault (Figure S2) (U.S. Dept. of Energy, Electric Power Research Institute, and U.S. Nuclear Regulatory Commission, 2012).

We estimate that the active Reelfoot fault length and rupture potential is a minimum of ~70 km, given the new minimum length of the 1812 event (58 km), the farthest extent of modern seismicity and coseismic sackungen, and diffuse geomorphic record of displacement (Figures 2, 5 and 8). The revised active fault trace is longer, extends farther south, and is mapped at a slightly different location and orientation than either current model trace (Figure S2). This longer fault length may impact hazard estimations if the entire 70-km-long Reelfoot fault ruptures, particularly if earthquake rupture continues on to the New Madrid West fault, as is currently depicted in one of the model scenarios (U.S. Dept. of Energy, Electric Power Research Institute, and U.S. Nuclear Regulatory Commission, 2012).

7. Conclusions

We document and measure deformed landforms in the Obion River valley in the New Madrid seismic zone using lidar and borehole data to constrain historical and late Quaternary slip along the Reelfoot fault. At least three terraces and two shoreline complexes record broad surficial folding across the projected trace of the blind Reelfoot fault. We compare surface profiles to stratigraphic data from three auger sites to demonstrate that apparent warping is not due to loess thickening and represents folding above a buried fault tip. These findings, combined with historical lake records, show that surface deformation from the 1812 earthquake extended southward through at least the Obion River valley, increasing the minimum 1812 rupture length to 58 km. The broad zone of surficial folding apparent in the Obion River valley dissipates farther south in the incised bluff terrain, but the total fault length is likely ≥70 km based on a continuation of modern seismicity and other geomorphic evidence of strong shaking, like sackungen. Additionally, progressive deformation across multiple terraces indicates a long-lived record of earthquakes that predates the existing paleoseismic record (~4 ka) and likely also predates ~24 ka. The folding observed in the Obion River valley is broader than fold scarps farther north along strike of the Reelfoot fault, which is consistent with models of a deep fault tip along this section of the fault. Together, these observations indicate that slip along the Reelfoot fault is continuous to the south, but slip is deeper and surface deformation is more diffuse and possibly diminished. The record of historical and prehistoric distributed, deep slip south of Reelfoot Lake has important implications for understanding slip potential and seismic hazard from the Reelfoot fault. Improved documentation of subtle tectonic signals from blind faulting, such as with high-resolution topographic data, is critical for characterizing seismic hazard in low strain, high erosion regions like the New Madrid seismic zone.

Data Availability Statement

Additional field data (auger descriptions, grain size results) are available from Delano et al. (2021). Lidar-derived DEMs and lidar point clouds are available at http://tngis.org/lidar and https://opentopography.org/, respectively.

Acknowledgments
Andrew Meigs, Stephen Angster, and an anonymous Tectonics reviewer provided critical reviews that improved this manuscript. The authors thank Jeff Nekola and Jeff Pigati for assistance identifying snails and Tina Dura for evaluating the presence/absence of diatoms. Jeff Biggs granted access to his property to auger. Map plate (Plate S1) and Figures S1 and S2 are available in the supporting information. The U.S. Geological Survey Earthquake Hazards Program and the Nuclear Regulatory Commission (NRC) supported this work. Findings presented in this study do not imply endorsement by the NRC. Any use of trade, product, or firm names is for descriptive purposes only and does not imply endorsement by the U.S. Government.

References

Autin, W. J., Burns, S. F., Miller, B. J., Saucier, R. T., & Snead, J. I. (1991). Quaternary geology of the Lower Mississippi Valley. In R. B. Morrison (Ed.), *Quaternary nonglacial geology, 547–582*. Geological Society of America. https://doi.org/10.1130/DNAG-

Bakun, W. H., & Hopper, M. G. (2004). Magnitudes and locations of the 1811-1812 New Madrid, Missouri, and the 1886 Charleston, South Carolina, earthquakes. *Bulletin of the Seismological Society of America*, (Vol. *94*, pp. 64–75). https://doi.org/10.1785/0120020122

Baldwin, J. N., Harris, J. B., Van Arsdale, R. B., Givler, R., Kelson, K. I., Sexton, J. L., & Lake, M. (2005). Constraints on the location of the late Quaternary Reelfoot and New Madrid North faults in the northern New Madrid seismic zone, central United States. *Seismological Research Letters*, *76*, 772–789. https://doi.org/10.1785/gssrl.76.6.772

Bullard, T. F., & Lettis, W. R. (1993). Quaternary fold deformation associated with blind thrust faulting, Los Angeles Basin, California. *Journal of Geophysical Research*, *98*, 8349–8369. https://doi.org/10.1029/93JB00012

Calais, E., Han, J. Y., DeMets, C., & Nocquet, J. M. (2006). Deformation of the North American plate interior from a decade of continuous GPS measurements: Deformation of North American plate. *Journal of Geophysical Research*, *111*, B06402. https://doi.org/10.1029/2005JB004253

Calais, E., & Stein, S. (2009). Time-variable deformation in the New Madrid seismic zone. *Science*, *323*, 1442. https://doi.org/10.1126/science.1168122

Carlson, S. D., & Guccione, M. J. (2010). Short-term uplift rates and surface deformation along the Reelfoot fault, New Madrid seismic zone. *Bulletin of the Seismological Society of America*, (Vol. *100*, pp. 1659–1677). https://doi.org/10.1785/0120100069

Center for Earthquake Research and Information. (2019). *New Madrid earthquake catalog*. Retrieved from http://folkworm.ceri.memphis.edu/catalogs/html/cat_nm.html

Champion, J., Mueller, K., Tate, A., & Guccione, M. (2001). Geometry, numerical models and revised slip rate for the Reelfoot fault and trishear fault-propagation fold, New Madrid seismic zone. *Engineering Geology*, (Vol. *62*, pp. 31–49). https://doi.org/10.1016/S0013-7952(01)00048-5

Conrad, T. A. (1856). Observations on the Eocene deposit of Jackson, Miss., with descriptions of 34 new species of shells and corals: Philadelphia Academy of Natural Science. *Proceedings*, *7*, 257–258.

Cox, R. T., Cherryhomes, J., Harris, J. B., Larsen, D., Van Arsdale, R. B., & Forman, S. L. (2006). Paleoseismology of the southeastern Reelfoot Rift in western Tennessee and implications for intraplate fault zone evolution. *Tectonics*, *25*, TC3019. https://doi.org/10.1029/2005TC001829

Crockett, D. (1834). *A narrative of the life of David Crockett, of the State of Tennessee*. Carey, Hart & Co.

Csontos, R., & Van Arsdale, R. (2008). New Madrid seismic zone fault geometry. *Geosphere*, *4*(5), 802–813. https://doi.org/10.1130/GES00141.1

Delano, J. E., Briggs, R. W., Thompson Jobe, J., Gold, R. D., & Engelhart, S. E. (2021). *Data to accompany the study "Quaternary Reelfoot fault deformation in the Obion River valley, Tennessee, USA"*. Geological Survey data release. https://doi.org/10.5066/P9GDM1VX

Delano, J. E., Gold, R. D., Briggs, R. W., & Jibson, R. W. (2018). Coseismic sackungen in the New Madrid seismic zone, USA. *Geophysical Research Letters*, *45*, 13258–13268. https://doi.org/10.1029/2018GL080493

DuRoss, C. B., Bunds, M. P., Gold, R. D., Briggs, R. W., Reitman, N. G., Personius, S. F., & Toké, N. A. (2019). Variable normal-fault rupture behavior, Northern Lost River Fault Zone, Idaho, USA. *Geosphere*, (Vol. *15*, pp. 1–24). https://doi.org/10.1130/GES02096.1

Fisk, H. N. (1944). *Geological investigations of the alluvial valley of the lower Mississippi* (p. 78). Mississippi River Commission.

Forman, S. L., Arthur Bettis, E., Kemmis, T. J., & Miller, B. B. (1992). Chronologic evidence for multiple periods of loess deposition during the late Pleistocene in the Missouri and Mississippi River Valley, United States: Implications for the activity of the Laurentide ice sheet. *Palaeogeography, Palaeoclimatology, Palaeoecology*, *93*, 71–83. https://doi.org/10.1016/0031-0182(92)90184-7

Forman, S. L., & Pierson, J. (2002). Late Pleistocene luminescence chronology of loess deposition in the Missouri and Mississippi River valleys, United States. *Palaeogeography, Palaeoclimatology. Palaeoecology*, *186*, 25–46. https://doi.org/10.1016/S0031-0182(02)00440-6

Fuller, M. L. (1912). The New Madrid earthquake. *U.S. Geological Survey Bulletin*, *494*, 119.

Gold, R. D., DuRoss, C. B., Delano, J. E., Jibson, R. W., Briggs, R. W., Mahan, S. A., et al. (2019). Four major Holocene earthquakes on the Reelfoot fault recorded by sackungen in the New Madrid seismic zone, USA. *Journal of Geophysical Research: Solid Earth*, *124*, 3105–3126. https://doi.org/10.1029/2018JB016806

Greenwood, M. L., Woolery, E. W., Van Arsdale, R. B., Stephenson, W. J., & Patterson, G. L. (2016). Continuity of the Reelfoot fault across the Cottonwood Grove and Ridgely faults of the New Madrid seismic zone. *Bulletin of the Seismological Society of America*, (Vol. *106*, pp. 2674–2685). https://doi.org/10.1785/0120150290

Hao, Y., Magnani, M. B., McIntosh, K., Waldron, B., & Guo, L. (2013). Quaternary deformation along the Meeman-Shelby Fault near Memphis, Tennessee, imaged by high-resolution marine and land seismic reflection profiles. *Tectonics*, *32*(3), 501–515. https://doi.org/10.1002/tect.20042

Holbrook, J., Autin, W. J., Rittenour, T. M., Marshak, S., & Goble, R. J. (2006). Stratigraphic evidence for millennial-scale temporal clustering of earthquakes on a continental-interior fault: Holocene Mississippi River Floodplain deposits New Madrid seismic zone, USA. *Tectonophysics*, (Vol. *420*, pp. 431–454). https://doi.org/10.1016/j.tecto.2006.04.002

Johnson, G. A., Horton, S. P., Withers, M., & Cox, R. (2014). Earthquake focal mechanisms in the New Madrid seismic zone. *Seismological Research Letters*, *85*(2), 257–267. https://doi.org/10.1785/0220130140

Johnston, A. C., & Schweig, E. S. (1996). The enigma of the New Madrid earthquakes of 1811–1812. *Annual Review of Earth and Planetary Sciences*, *24*(1), 339–384. https://doi.org/10.1146/annurev.earth.24.1.339

Kelson, K. I., Simpson, G. D., Van Arsdale, R. B., Haraden, C. C., & Lettis, W. R. (1996). Multiple late Holocene earthquakes along the Reelfoot fault, central New Madrid seismic zone. *Journal of Geophysical Research*, *101*, 6151–6170. https://doi.org/10.1029/95JB01815

Leigh, D. S., & Knox, J. C. (1993). AMS radiocarbon age of the upper Mississippi Valley Roxana Silt. *Quaternary Research*, *39*, 282–289. https://doi.org/10.1006/qres.1993.1035

Lyell, C. (1849). *A second visit to the United States of North America. New York*. Harper & Brothers, Publishers. John Murray. [Pdf] Retrieved from the Library of Congress. https://www.loc.gov/item/01026866/

Markewich, H. W., Wysocki, D. A., Pavich, M. J., Rutledge, E. M., Millard, H. T., Rich, F. J., et al. (1998). Paleopedology plus TL, ^{10}Be, and ^{14}C dating as tools in stratigraphic and paleoclimatic investigations, Mississippi River Valley, U.S.A. *Quaternary International*, *51–52*, 143–167. https://doi.org/10.1016/S1040-6182(97)00041-4

Martin, S. S., & Hough, S. E. (2019). Where was the 31 October 1895 Charleston, Missouri, earthquake? *Bulletin of the Seismological Society of America*, *109*(4), 1479–1497. https://doi.org/10.1785/0120180328

McKay, E. D. (1979). Wisconsin loess stratigraphy of Illinois. *Illinois State Geological Survey Guidebook*, *13*, 95–108.

Meigs, A. (2013). Active tectonics and the LiDAR revolution. *Lithosphere*, (Vol. *5*, pp. 226–229). https://doi.org/10.1130/RF.L004.1

Mueller, K., & Pujol, J. (2001). Three-dimensional geometry of the Reelfoot blind thrust: Implications for moment release and earthquake magnitude in the New Madrid seismic zone. *Bulletin of the Seismological Society of America*, *91*, 1563–1573. https://doi.org/10.1785/0120000276

Nekola, J. C., & Pigati, J. S. (2018). *Snail identification, written communication*.

Nuttli, O. W. (1973). The Mississippi Valley earthquakes of 1811 and 1812: Intensities, ground motion and magnitudes. *Bulletin of the Seismological Society of America*, *63*, 227–248.

Olson, P. L., Legg, N. T., Abbe, T. B., Reinhart, M. A., & Radloff, J. K. (2014). *A methodology for delineating planning-level channel migration zones* (p. 83). Washington State Department of Ecology.

Petersen, M. D., Moschetti, P. M., Mueller, C. S., Haller, K. M., Frankel, A. D., Zeng, Y., et al. (2014). Documentation for the 2014 update of the United States national seismic hazard maps. *U.S. Geological Survey Open-File Report 2014–, 1091*, 243.

Pigati, J. S., McGeehin, J. P., Muhs, D. R., Grimley, D. A., & Nekola, J. C. (2015). Radiocarbon dating loess deposits in the Mississippi Valley using terrestrial gastropod shells (Polygyridae, Helicinidae, and Discidae). *Aeolian Research*, *16*, 25–33. https://doi.org/10.1016/j.aeolia.2014.10.005

Pratt, T. L. (2012). Kinematics of the New Madrid seismic zone, central United States, based on stepover models. *Geology*, *40*, 371–374. https://doi.org/10.1130/G32624.1

Reimer, P. J., Austin, W. E. N., Bard, E., Bayliss, A., Blackwell, P. G., Bronk Ramsey, C., et al. (2020). The IntCal20 northern hemisphere radiocarbon age calibration curve (0–55 cal kBP). *Radiocarbon*, *62*(4), 725–757. https://doi.org/10.1017/RDC.2020.41

Rhea, M. (1832). *Map of the state of Tennessee taken from survey. Columbia, Tenn Matthew Rhea*. Retrieved from https://www.loc.gov/item/2011588000/

Rittenour, T. M., Blum, M. D., & Goble, R. J. (2007). Fluvial evolution of the lower Mississippi River valley during the last 100 k.y. glacial cycle: Response to glaciation and sea-level change. *GSA Bulletin*, *119*, 586–608. https://doi.org/10.1130/B25934.1

Rodbell, D. T. (1996). Subdivision, subsurface stratigraphy, and estimated age of fluvial-terrace deposits in northwestern Tennessee. *U.S. Geological Survey Bulletin*, *2128*, 24. https://doi.org/10.3133/b2128

Rodbell, D. T., Forman, S. L., Pierson, J., & Lynn, W. C. (1997). Stratigraphy and chronology of Mississippi Valley loess in western Tennessee. *GSA Bulletin*, *109*, 1134–1148. https://doi.org/10.1130/0016-7606(1997)109<1134:SACOMV>2.3.CO;2

Rodbell, D. T., & Schweig, E. S. (1993). The record of seismically induced liquefaction on late Quaternary terraces in northwestern Tennessee. *Bulletin of the Seismological Society of America*, *83*, 269–278.

Ruhe, R. V. (1983). Depositional environment of late Wisconsin loess in the midcontinental United States. In S. C. Porter (Ed.), *Late-Quaternary Environments of the United States, the Late Pleistocene* (Vol. 1, pp. 130–137). University of Minnesota Press.

Russ, D. P. (1979). Late Holocene faulting and earthquake recurrence in the Reelfoot Lake area, northwestern Tennessee. *The Geological Society of America Bulletin*, *90*(11), 1013–1018. https://doi.org/10.1130/0016-7606(1979)90<1013:LHFAER>2.0.CO;2

Russ, D. P. (1982). Style and significance of surface deformation in the vicinity of New Madrid, Missouri: Investigations of the New Madrid, Missouri, earthquake region. *U. S. Geological Survey Professional Paper*, (Vol. *1236*, pp. 95–114).

Russell, J. (1795). *Map of the southern states of America, Comprehending Maryland, Virginia, Kentucky, Territory s'th: Of the Ohio, Tennessee Governm't North Carolina South Carolina, & Georgia*.

Saucier, R. T. (1987). Geomorphological interpretations of late Quaternary terraces in western Tennessee and their regional tectonic implications. *U. S. Geological Survey Professional Paper*, (Vol. *1336*, p. 19).

Saucier, R. T., & Fleetwood, A. R. (1970). Origin and chronologic significance of late Quaternary terraces, Ouachita River, Arkansas and Louisiana. *The Geological Society of America Bulletin*, *81*(3), 869–890. https://doi.org/10.1130/0016-7606(1970)81[869:OACSOL]2.0.CO;2

Shankman, D., & Samson, S. A. (1991). Channelization effects on Obion River flooding, western Tennessee. *Journal of the American Water Resources Association*, *27*, 247–254. https://doi.org/10.1111/j.1752-1688.1991.tb03129.x

Simon, A., & Hupp, C. R. (1992). Geomorphic and vegetative recovery processes along modified stream channels of West Tennessee. *U.S. Geological Survey Open-File. Report 91–502*. https://doi.org/10.3133/ofr91502

Snowden, J. O., & Priddy, R. R. (1968). *Loess investigations in Mississippi: Mississippi geological, economic, and topographic survey bulletin 111*.

Stahle, D. W., Van Arsdale, R. B., & Cleaveland, M. K. (1992). Tectonic signal in baldcypress trees at Reelfoot Lake, Tennessee. *Seismological Research Letters*, *63*(3), 439–447. https://doi.org/10.1785/gssrl.63.3.439

Stephenson, W. J., Shedlock, K. M., & Odum, J. K. (1995). *Characterization of the Cottonwood Grove and Ridgely faults near Reelfoot Lake, Tennessee, from high-resolution seismic reflection data*. (Report No. 1538I). https://doi.org/10.3133/pp1538I

Stuiver, M., Reimer, P. J., & Reimer, R. W. (2021). *CALIB 8.2*. Retrieved from http://calib.org

Thompson Jobe, J. A., Gold, R. D., Briggs, R. W., Williams, R. A., Stephenson, W. J., Delano, J. E., et al. (2020). Evidence for late Quaternary deformation along Crowleys Ridge, New Madrid seismic zone. *Tectonics*, *39*, e2019TC005746. https://doi.org/10.1029/2019TC005746

Tuttle, M. P., Schweig, E. S., Campbell, J., Thomas, P. M., Sims, J. D., & Lafferty, R. H. (2005). Evidence for New Madrid earthquakes in A.D. 300 and 2350 B.C. *Seismological Research Letters*, *76*(4), 489–501. https://doi.org/10.1785/gssrl.76.4.489

Tuttle, M. P., Schweig, E. S., Sims, J. D., Lafferty, R. H., Wolf, L. W., & Haynes, M. L. (2002). The earthquake potential of the New Madrid seismic zone. *Bulletin of the Seismological Society of America*, *92*(6), 2080–2089. https://doi.org/10.1785/0120010227

Tuttle, M. P., Wolf, L. W., Starr, M. E., Villamor, P., Lafferty, R. H., Morrow, J. E., et al. (2019). Evidence for Large New Madrid Earthquakes about A.D. 0 and 1050 B.C., Central United States. *Seismological Research Letters*, *90*(3), 1393–1406. https://doi.org/10.1785/0220180371

USACE. (2012). *Western Tennessee lidar*. Retrieved from https://www.tn.gov/finance/sts-gis/gis/gis-projects/gis-projects-elevation.html

U.S. Dept. of Energy, Electric Power Research Institute, and U.S. Nuclear Regulatory Commission. (2012). *Central and eastern United States seismic source characterization for nuclear facilities: NUREG-2115* (p. 112). Retrieved from https://www.nrc.gov/docs/ML1204/ML12048A804.pdf

U.S. Fish and Wildlife Service. (1989). *Reelfoot Lake water level management: Final environmental impact statement*. GA.

U.S Geological Survey. (2014). *New Madrid seismic zone*: Central U.S. ARRA lidar. https://doi.org/10.5069/G9N014G4

Van Arsdale, R., Pryne, D., & Woolery, E. (2013). Northwestern extension of the Reelfoot North fault near New Madrid, Missouri. *Seismological Research Letters*, *84*(6), 1114–1123. https://doi.org/10.1785/0220130067

Van Arsdale, R., Purser, J., Stephenson, W., & Odum, J. (1998). Faulting along the southern margin of Reelfoot Lake, Tennessee. *Bulletin of the Seismological Society of America*, *88*, 131–139.

Van Arsdale, R. B., Cox, R. T., Johnston, A. C., Stephenson, W. J., & Odum, J. K. (1999). Southeastern extension of the Reelfoot fault. *Seismological Research Letters*, *70*(3), 348–359. https://doi.org/10.1785/gssrl.70.3.348

Van Arsdale, R. B., Kelson, K. I., & Lumsden, C. H. (1995). Northern extension of the Tennessee Reelfoot scarp into Kentucky and Missouri. *Seismological Research Letters*, *66*(5), 57–62. https://doi.org/10.1785/gssrl.66.5.57

Vogel, J. S., Southon, J. R., Nelson, D. E., & Brown, T. A. (1984). Performance of catalytically condensed carbon for use in accelerator mass spectrometry. *Nuclear Instruments and Methods in Physics Research B 5*, 289–293. https://doi.org/10.1016/0168-583x(84)90529-9

Wentworth, C. K. (1922). A scale of grade and class terms for clastic sediments. *The Journal of Geology*, *30*, 377–392. https://doi.org/10.1086/622910